Journal of Statistical Mechanics:
Theory and Experiment

PAPER: CLASSICAL STATISTICAL MECHANICS, EQUILIBRIUM AND NON-EQUILIBRIUM

Long-wavelength instabilities in a system of interacting active particles

Journal of Statistical Mechanics: Theory and Experiment
An IOP and SISSA journal

PAPER: Classical statistical mechanics, equilibrium and non-equilibrium

Long-wavelength instabilities in a system of interacting active particles

Zahra Fazli[1] **and Ali Najafi**[1,2]

[1] Department of Physics, Institute for Advanced Studies in Basic Sciences (IASBS), Zanjan 45137-66731, Iran
[2] Research Center for Basic Sciences and Modern Technologies (RBST), Institute for Advanced Studies in Basic Sciences (IASBS), Zanjan 45137-66731, Iran
E-mail: najafi@iasbs.ac.ir

Received 30 September 2017
Accepted for publication 26 December 2017
Published 8 February 2018

Online at stacks.iop.org/JSTAT/2018/023201
https://doi.org/10.1088/1742-5468/aaa795

Abstract. Based on a microscopic model, we develop a continuum description for a suspension of microscopic self-propelled particles. With this continuum description we study the role of long-range interactions in destabilizing macroscopic ordered phases that are developed by short-range interactions. Long-wavelength fluctuations can destabilize both isotropic and symmetry-broken polar phases in a suspension of dipolar particles. The instabilities in a suspension of pullers (pushers) arise from splay (bend) fluctuations. Such instabilities are not seen in a suspension of quadrupolar particles.

Keywords: active matter, biological fluid dynamics, Brownian motion

J. Stat. Mech. (2018) 023201

1742-5468/18/023201+29$33.00

Contents

1. Introduction

The dynamics of a suspension of interacting active particles, as a non-equilibrium problem in statistical mechanics, has attracted considerable interest in recent years [1–4]. Systems like schools of fish and birds [5–7], bacterial colonies [8–11], gels of bio-polymers [12] and interacting active Janus particles [13–15] show a wide range of fascinating physical behavior. Coherent collective motions, long-range orientational order [16, 17], large-number fluctuations and pattern formations are examples of such phenomena [8, 16, 18].

At first glance, the long-range order observed in two-dimensional active systems seems to be in contrast with the Mermin–Wagner theorem, which states that spontaneous breaking of continuous symmetries is impossible in low-dimensional equilibrium systems with sufficiently short-range interactions. The lack of such symmetry breaking is due to the divergence of spin-wave-like fluctuations that must appear after symmetry breaking in equilibrium systems [19]. But a theoretical work based on renormalization group analysis by Toner and Tu has revealed a physical scenario in which the non-equilibrium nature of active systems can provide conditions for the appearance of the

J. Stat. Mech. (2018) 023201

true order in lower dimensions [20]. However, as a result of long-range hydrodynamic interaction between particles, orientational order in a wet active system is inevitably unstable [21–24]. The mechanism and origin of this hydrodynamically mediated dynamical instability are different from the fluctuation divergence that follows a symmetry breaking in low-dimensional equilibrium systems. Hydrodynamically mediated instability is a non-universal size-dependent phenomenon and it is sensitive to the microscopic details of swimming strokes [25–27].

Long-wavelength instabilities in both dry and wet active systems have been studied using different approaches [28–35].

In addition to numerical studies [36–40], continuum descriptions can provide analytical tools for dealing with such non-equilibrium systems. Microscopic derivations [30–32, 41, 42] and symmetry arguments [20, 43–45] are two approaches that can provide the governing equations for macroscopic continuum fields. In this article we aim to use a microscopic approach and obtain the equations of macroscopic description. The continuum description derived from the microscopic model in this article will allow us to study the role of long-range interactions in instabilities observed in active suspensions. To take into account the hydrodynamic interactions between swimmers, we will use an effective treatment whereby at the level of two swimmers, we eliminate the fluid degrees of freedom from the fluid–swimmer coupled equations and obtain effective interaction between swimmers. Our approach is different from the method used in [44], where the swimmer's activity enters through an active stress into the hydrodynamic equations by a coarse-graining procedure. Our approach is similar to a work that considered the dynamics of a suspension confined in two dimensions [46].

Theories based on symmetry arguments reveal qualitative features of long-wavelength instabilities in active suspensions. Microscopic-based models can help us to understand the origin of instabilities more quantitatively. We will show that both isotropic and polar phases that can appear in active systems are unstable with respect to long-wavelength fluctuations.

The structure of this article is as follows: in section 2, we present the hydrodynamic details of our microscopic model and introduce long- and short-range interactions between swimmers. Then in section 3, we describe the dynamics of a suspension of many swimmers in terms of Langevin and Smoluchowski descriptions. Furthermore, we simplify the description by considering mean-field approximation. In section 4, we derive a continuum description for the system. Dynamical equations, their steady-state solutions and instability analysis are presented in this section. Finally, a discussion and a summary are presented in section 5.

2. Hydrodynamic model for micro-swimmers

We start with a microscopic model for a minimal autonomous micro-swimmer that can propel itself in aqueous media. Theoretical arguments based on symmetry grounds show that a minimum number of two internal degrees of freedom is necessary to capture the hydrodynamic details of a micro-swimmer [47]. To construct the model swimmer, consider three spheres with radii a, connected linearly by two arms with variable

J. Stat. Mech. (2018) 023201

lengths given by $L^{\rm f}$ and $L^{\rm b}$. We label the spheres f (front), b (back) and m (middle). It is shown that harmonic changes in the arm lengths with a phase lag between the arms will result in a non-zero swimming velocity for this system [48, 49]. To see how the above swimmer works, one needs to solve the hydrodynamic equations for the ambient fluid that are coupled to the motion of the spheres. On the micrometer scale with a velocity range about micrometers per second in water, the linear Stokes equation governs the dynamics of the fluid. Assuming that the arms are thin enough to neglect their hydrodynamic effects and eliminating the fluid degrees of freedom, one can obtain the effective equations that govern the dynamics of the spheres alone. Such equations are linear relations between the velocity of the spheres and the hydrodynamic forces exerted by the spheres on the fluid [50]:

$$v_i^m = \sum_{j,n} O_{ij}^{mn}\, f_j^n, \tag{1}$$

where f_j^n (v_j^n) denotes the jth component of the force (velocity) of sphere n and the details of the hydrodynamic interactions are given by the kernel O_{ij}^{mn}. This hydrodynamic kernel is a function of the size of the spheres and their relative position. Denoting the distance between spheres m and n by $\mathbf{d} = \mathbf{x}^m - \mathbf{x}^n$ and the fluid viscosity by η and in the limit of $d \gg a$, Oseen's tensor provides an approximation for the hydrodynamic kernel [50]:

$$O_{ij}^{mn} = \begin{cases} \frac{1}{8\pi\eta d}\left(\delta_{ij} + \hat{d}_i\hat{d}_j\right) & \text{for } m \neq n \\ \frac{\delta_{ij}}{6\pi\eta a} & \text{for } m = n \end{cases}. \tag{2}$$

As the swimmer is autonomous, one needs to add the conditions of zero total force and zero total torque to the above dynamical equations. The above relations and the constraints that prescribe the dynamics of the arm lengths provide a complete set of dynamical equations that can fully determine the state of the swimmer, including its speed, direction and forces. The velocities and forces averaged over time are the quantities that we are interested to know. To express the results, let us assume that the arms oscillate around a mean value ℓ:

$$L^{\rm f}(t) = \ell + u^{\rm f}(t), \qquad L^{\rm b}(t) = \ell(1+\delta) + u^{\rm b}(t), \tag{3}$$

where $u^{\rm f}$ and $u^{\rm b}$ are periodic functions of time and δ is a parameter that makes the swimmer geometrically asymmetric. After solving the above equations, the average swimming velocities (linear and angular) and forces acting on the fluid read as [49]:

$$\mathbf{v}_0 = v_0\,\hat{\mathbf{t}}, \qquad \mathbf{\Omega}_0 = 0 \tag{4}$$

$$\langle \mathbf{f}^{\rm f}\rangle = -\frac{5}{4}\pi\eta\left(\frac{a}{\ell}\right)^2\left(1 - \frac{17}{5}\delta\right)\Phi\,\hat{\mathbf{t}},\ \langle \mathbf{f}^{\rm b}\rangle = -\frac{5}{4}\pi\eta\left(\frac{a}{\ell}\right)^2\left(1 + \frac{7}{5}\delta\right)\Phi\,\hat{\mathbf{t}}, \tag{5a}$$

where $v_0 = -\frac{7}{12}\left(\frac{a}{\ell^2}\right)(1-\delta)\Phi$, $\hat{\mathbf{t}}$ represents the direction of the swimmer and $\Phi = \langle u^{\rm f}\dot{u}^{\rm b}\rangle$ with $\langle\ldots\rangle$ shows the averaging over time. Additionally $\langle \mathbf{f}^{\rm m}\rangle = -\langle \mathbf{f}^{\rm b}\rangle - \langle \mathbf{f}^{\rm f}\rangle$. In writing the above results, we assume that $a \ll \ell$, $u^{\rm f} \ll \ell$, $u^{\rm b} \ll \ell$ and $\delta \ll 1$. Throughout this paper we choose $\Phi < 0$, so that $v_0 > 0$.

J. Stat. Mech. (2018) 023201

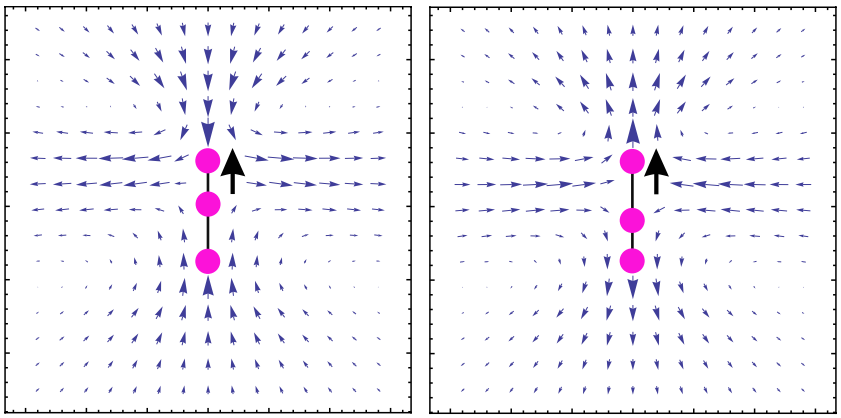

Figure 1. Velocity fields of a puller (left) and a pusher (right). In both cases, the swimmer moves upward, along the bold arrow. The velocity field decreases with $1/r^2$.

When considering the force distribution of a swimmer, the asymmetry parameter δ plays an essential role. For a symmetric swimmer ($\delta = 0$), the force distribution shows a quadrupolar field while for the asymmetric case ($\delta \neq 0$) it shows a dipolar field [51]. Defining the force dipole tensor as $\Gamma_{ij} = \sum_m x_i^m f_j^m$, we can calculate it as:

$$\mathbf{\Gamma} = -\frac{29}{10} f_0 \, \ell \, \delta \, \hat{\mathbf{t}}\hat{\mathbf{t}}, \tag{6}$$

where $f_0 = \frac{30}{7}\pi\eta a v_0$. Based on the observation that the driving force of the motion is located at the head or at the tail of the swimmer, we can divide dipolar swimmers into two categories of pushers and pullers. For pushers, the driving force comes from the tail while for pullers, the driving force comes from the head. In an asymmetric three-sphere swimmer with $\Phi < 0$, $\delta > 0$ corresponds to a puller ($\Gamma_{tt} < 0$) and $\delta < 0$ results in a pusher ($\Gamma_{tt} > 0$). For a puller (pusher), the back (front) arm of the swimmer is longer than the front (back) arm. Figure 1 shows the flow field pattern for both pusher and puller. There is a fundamental difference between the flow patterns for pushers and pullers. In the next sections we will see that the hydrodynamic interaction between the swimmers crucially depends on the sign of δ.

2.1. Long-range interactions

Since we want to consider a suspension of micro-swimmers, we need to calculate the hydrodynamic interactions between them. The above model of a micro-swimmer allows us to obtain an analytic formula for the interactions. The details of such calculations are similar to the case of a single swimmer and have been studied elsewhere [52, 53]. Here we only present the final results. Consider two swimmers located at positions $\mathbf{r}$ and $\mathbf{r}'$ with orientations given by $\hat{\mathbf{t}}$ and $\hat{\mathbf{t}}'$. Taking into account the hydrodynamic long-range interactions between the swimmers, the linear and angular velocities of the first swimmer averaged over the oscillations of both swimmers read as:

$$\mathbf{V}^{\mathrm{L}}\left(\mathbf{r}, \mathbf{r}', \hat{\mathbf{t}}, \hat{\mathbf{t}}'\right) = a_1 \left(\frac{\ell}{R}\right)^2 \mathbf{G}_1 + \left(\frac{\ell}{R}\right)^3 \left(a_2 \, \mathbf{G}_2 + a_3 \, \mathbf{G}_3\right), \tag{7}$$

J. Stat. Mech. (2018) 023201

$$\mathbf{\Omega}^{\mathrm{L}}\left(\mathbf{r},\mathbf{r}',\hat{\mathbf{t}},\hat{\mathbf{t}}'\right)=a_4\left(\frac{\ell}{R}\right)^3\mathbf{G}_4+\left(\frac{\ell}{R}\right)^4\left(a_5\,\mathbf{G}_5+a_6\,\mathbf{G}_6\right), \tag{8}$$

where $\mathbf{R}=\mathbf{r}-\mathbf{r}'$ and superscript L denotes long-range interaction. The coefficients are given by:

$$\begin{aligned} a_1&=-\frac{87}{56}\left(\frac{a}{\ell}\right)\delta v_0, \qquad a_2=-\frac{6}{7}\left(2+\delta\right)v_0, \qquad a_3=-\frac{1}{2}a_2,\\ a_4&=-\frac{1}{\ell}a_1, \qquad a_5=-\frac{1}{\ell}a_2, \qquad a_6=\frac{3}{2}\left(\frac{1}{\ell}\right)\left(2-\delta\right)v_0. \end{aligned} \tag{9}$$

Regarding the above results for the interactions, the terms proportional to a_1 and a_4 represent the dipolar contributions and the other terms show the quadrupolar contributions. Vectors $\mathbf{G}_1,\cdots,\mathbf{G}_6$ are functions of the relative displacement and orientation of the swimmers, given by:

$$\mathbf{G}_1=-3M_{ij}(\hat{\mathbf{R}})\,\hat{t}_i'\hat{t}_j'\hat{\mathbf{R}}, \tag{10}$$

$$\mathbf{G}_2=\frac{3}{2}M_{ij}(\hat{\mathbf{R}})\,\hat{t}_i'\hat{t}_j'\hat{\mathbf{t}}'+\frac{3}{2}M_{ijk}(\hat{\mathbf{R}})\,\hat{t}_i'\hat{t}_j'\hat{t}_k'\hat{\mathbf{R}}, \tag{11}$$

$$\mathbf{G}_3=-3M_{ij}(\hat{\mathbf{R}})\,\hat{t}_i'\hat{t}_j'\hat{\mathbf{t}}+3M_{ijk}(\hat{\mathbf{R}})\,\hat{t}_i'\hat{t}_j'\hat{t}_k\hat{\mathbf{R}}, \tag{12}$$

$$\mathbf{G}_4=3M_{ijk}(\hat{\mathbf{R}})\,\hat{t}_i'\hat{t}_j'\hat{t}_k\hat{\mathbf{R}}, \tag{13}$$

$$\mathbf{G}_5=\frac{3}{2}M_{ijk}(\hat{\mathbf{R}})\,\hat{t}_i'\hat{t}_j'\hat{t}_k\hat{\mathbf{t}}'-\frac{15}{2}M_{ijkl}(\hat{\mathbf{R}})\,\hat{t}_i'\hat{t}_j'\hat{t}_k'\hat{t}_l\hat{\mathbf{R}}, \tag{14}$$

$$\mathbf{G}_6=-\frac{15}{2}M_{ijkl}(\hat{\mathbf{R}})\,\hat{t}_i'\hat{t}_j'\hat{t}_k\hat{t}_l\hat{\mathbf{R}}, \tag{15}$$

where summation over repeated indices is assumed and

$$\begin{aligned} M_{ij}(\hat{\mathbf{R}})&=\hat{R}_i\hat{R}_j-\frac{1}{3}\,\delta_{ij}, \qquad M_{ijk}(\hat{\mathbf{R}})=-R^4\partial_k\left(\frac{M_{ij}}{R^3}\right),\\ M_{ijkl}(\hat{\mathbf{R}})&=-\frac{R^5}{5}\partial_l\left(\frac{M_{ijk}}{R^4}\right), \end{aligned} \tag{16}$$

where we use the shorthand notation $\partial_i=\partial/\partial R_i$. To obtain the above hydrodynamic interactions, we assume that the swimmers are very far, $R\gg\ell$, and we also average over the internal motion of the swimmers. As seen from equations (7) and (8), the first non-zero terms in the hydrodynamic interaction, the terms that are proportional to $(\frac{\ell}{R})^2$ in linear velocity and $(\frac{\ell}{R})^3$ in rotational velocity, are proportional to δ. This is the contribution from the dipolar field of the asymmetric swimmers. Such contribution changes signs for pushers and pullers [54–56].

In the above equations, we use a compact notation for the interaction terms. An alternative representation given in appendix B can reveal the physical picture behind each term. As a result of that representation, different terms in equations (7) and (8) can be considered as flow fields due to some hydrodynamic singularities like a force

J. Stat. Mech. (2018) 023201

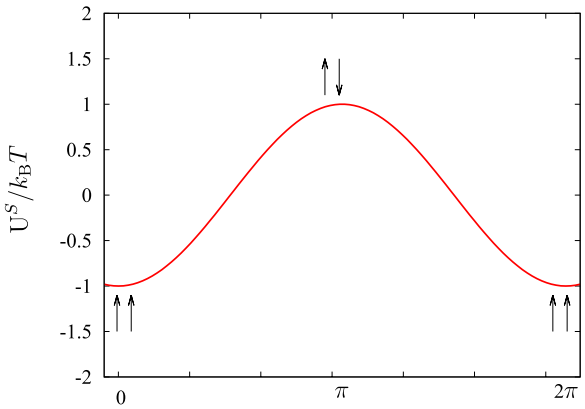

Figure 2. Short-range alignment interaction, U^S, between the swimmers is plotted as a function of the angle between their orientations. The potential has a minimum when two swimmers are aligned. Here we assume $U_0 = 1$.

dipole, a source dipole and higher-order multipoles. The change in the velocity of the first swimmer can be considered as the flow of singularities located at the position of the second swimmer and calculated at the position of the first swimmer. For example the term proportional to a_1 shows the flow of a force dipole and the a_2 term contains a source dipole and a force quadrupole.

Rich dynamical behavior that includes coherent motion in two interacting swimmers suggests we could see interesting phases in a system with many interacting swimmers [53, 57]. In the next sections we will see how the thermodynamic behavior of a suspension of micro-swimmers depends on the nature of two-particle interactions.

2.2. Short-range interactions

As one can see from equations (7) and (8), the long-range hydrodynamic interactions that we have obtained are valid only at large distances: they diverge at short distances. Due to the complexity of hydrodynamics at short distances, it is not possible to obtain simple analytic results for the short-range part of the interactions. We can use an approximate phenomenological model that takes into account the short-range part of the interactions. Inspired by the well-known Vicsek model [39], we consider a short-range ferromagnetic interaction potential as:

$$\mathrm{U}^{\mathrm{S}}(\mathbf{r},\mathbf{r}',\hat{\mathbf{t}},\hat{\mathbf{t}}') = \begin{cases} -k_{\mathrm{B}}TU_0\,\hat{\mathbf{t}}\cdot\hat{\mathbf{t}}' & \text{for } R \leqslant \ell_{\mathrm{c}}, \\ 0 & \text{for } R > \ell_{\mathrm{c}} \end{cases} \tag{17}$$

where ℓ_{c} is a crossover length scale that separates short- and long-range interactions. We assume that long-range hydrodynamic interactions act only for swimmers having distances larger than ℓ_{c}. As seen from figure 2, the above potential tends to align nearby particles. The crossover length ℓ_{c} has the same order of magnitude as the linear dimension of the swimmers given by 2ℓ. It should be mentioned that the above interaction does not consider all information on short-range interactions in real systems; this model only takes into account the steric interaction between nearby swimmers. In terms of potential energy, the short-range velocities can be written as:

$$\mathbf{V}^{\mathrm{S}}(\mathbf{r},\mathbf{r}',\hat{\mathbf{t}},\hat{\mathbf{t}}') = -\frac{1}{k_{\mathrm{B}}T}\,\mathbf{D}\cdot\boldsymbol{\nabla}\mathrm{U}^{\mathrm{S}}, \tag{18}$$

$$\boldsymbol{\Omega}^{\mathrm{S}}(\mathbf{r},\mathbf{r}',\hat{\mathbf{t}},\hat{\mathbf{t}}') = -\frac{D_{\mathrm{R}}}{k_{\mathrm{B}}T}\,\boldsymbol{\nabla}_{\mathrm{R}}\mathrm{U}^{\mathrm{S}}, \tag{19}$$

where $\boldsymbol{\nabla}$ and $\boldsymbol{\nabla}_{\mathrm{R}} \equiv \hat{\mathbf{t}}\times\partial/\partial\hat{\mathbf{t}}$ are the translational and rotational gradient operators. In some previous studies concerning continuum description [30, 31], a Vicsek-like short-range alignment interaction for a collection of point particles has been considered. The Boltzmann–Ginzburg–Landau approach used in [30] considered both ferromagnetic and nematic short-range ordering and in [31], which is based on an Enskog-type kinetic theory, a ferromagnetic interaction was considered. The ferromagnetic interaction that we consider in this article introduces a polar order in the system.

In the above equations, $\mathbf{D}$ is the translational diffusion tensor of a micro-swimmer and for a swimmer with elongated geometry we can decompose it into its parallel, $D_{\parallel}$, and perpendicular, $D_{\perp}$, components:

$$\mathrm{D}_{ij} = D_{\parallel}\hat{t}_i\hat{t}_j + D_{\perp}\left(\delta_{ij} - \hat{t}_i\hat{t}_j\right), \tag{20}$$

and D_{R} is the rotational diffusion coefficient. Through hydrodynamic calculations, we can obtain the translational and rotational diffusion coefficients [58, 59].

The details of such calculations are presented in appendix A. The final results are:

$$D_{\parallel} = \frac{k_{\mathrm{B}}T}{18\pi\eta a}\left[1 + \frac{5}{2}\left(1-\frac{\delta}{2}\right)\left(\frac{a}{\ell}\right) + \mathcal{O}\left(\frac{a}{\ell}\right)^2\right], \tag{21}$$

$$D_{\perp} = \frac{k_{\mathrm{B}}T}{18\pi\eta a}\left[1 + \frac{5}{4}\left(1-\frac{\delta}{2}\right)\left(\frac{a}{\ell}\right) + \mathcal{O}\left(\frac{a}{\ell}\right)^2\right], \tag{22}$$

$$D_{\mathrm{R}} = \frac{k_{\mathrm{B}}T}{12\pi\eta a\,\ell^2}\left[(1-\delta) - \frac{3}{8}\left(1-\frac{3}{2}\delta\right)\left(\frac{a}{\ell}\right) + \mathcal{O}\left(\frac{a}{\ell}\right)^2\right]. \tag{23}$$

3. Dynamics of a suspension

3.1. Langevin dynamics

Let us consider a dilute suspension of $\mathcal{N}$ micro-swimmers moving in a three-dimensional fluid medium with temperature T. To describe the dynamics of the suspension, we can start with Langevin description for each micro-swimmer:

$$\partial_t\mathbf{r}_\alpha = v_0\,\hat{\mathbf{t}}_\alpha + \sum_{\beta\neq\alpha}\mathbf{V}^{\mathrm{int}}\left(\mathbf{r}_\alpha,\mathbf{r}_\beta,\hat{\mathbf{t}}_\alpha,\hat{\mathbf{t}}_\beta\right) + \boldsymbol{\eta}^{\mathrm{T}}_\alpha(t), \tag{24}$$

$$\partial_t\hat{\mathbf{t}}_\alpha = \sum_{\beta\neq\alpha}\boldsymbol{\Omega}^{\mathrm{int}}\left(\mathbf{r}_\alpha,\mathbf{r}_\beta,\hat{\mathbf{t}}_\alpha,\hat{\mathbf{t}}_\beta\right)\times\hat{\mathbf{t}}_\alpha + \boldsymbol{\eta}^{\mathrm{R}}_\alpha(t), \tag{25}$$

J. Stat. Mech. (2018) 023201

where $\mathbf{r}_\alpha$ denotes the position vector for the hydrodynamic center of the αth swimmer ($\alpha = 1, \ldots, \mathcal{N}$) and $\hat{\mathbf{t}}_\alpha$ its director. The hydrodynamic center is defined in the appendix. In the above relation the summation is over all other swimmers ($\beta \neq \alpha$). $\mathbf{V}^{\text{int}}$ and $\mathbf{\Omega}^{\text{int}}$ are the interaction contributions to the translational and rotational velocities of the swimmers. We consider two types of interactions between the swimmers: a short-range alignment interaction and a long-range one that is due to the fluid-mediated interactions between the swimmers. So $\mathbf{V}^{\text{int}}$ and $\mathbf{\Omega}^{\text{int}}$ contain two terms:

$$\mathbf{V}^{\text{int}}\left(\mathbf{r}_\alpha, \mathbf{r}_\beta, \hat{\mathbf{t}}_\alpha, \hat{\mathbf{t}}_\beta\right) = \mathbf{V}^{\text{L}} + \mathbf{V}^{\text{S}}, \tag{26}$$

$$\mathbf{\Omega}^{\text{int}}\left(\mathbf{r}_\alpha, \mathbf{r}_\beta, \hat{\mathbf{t}}_\alpha, \hat{\mathbf{t}}_\beta\right) = \mathbf{\Omega}^{\text{L}} + \mathbf{\Omega}^{\text{S}}. \tag{27}$$

Recall that in the last section we have obtained the long- and short-range parts of the interaction. $\boldsymbol{\eta}^{\text{T}}_\alpha(t)$ and $\boldsymbol{\eta}^{\text{R}}_\alpha(t)$ are stochastic terms due to random forces which swimmer α receives from the molecules of the ambient fluid. The random forces obey the statistics of Gaussian noise:

$$\langle \eta^{\text{T}}_{\alpha,i}(t)\eta^{\text{T}}_{\beta,j}(t')\rangle = \text{D}_{ij}\,\delta_{\alpha\beta}\,\delta(t-t'), \tag{28}$$

$$\langle \eta^{\text{R}}_{\alpha,i}(t)\eta^{\text{R}}_{\beta,j}(t')\rangle = D_{\text{R}}\,\delta_{ij}\,\delta_{\alpha\beta}\,\delta(t-t'). \tag{29}$$

3.2. Statistical description

In order to obtain a probabilistic description for a suspension composed of $\mathcal{N}$ particles, we denote the $\mathcal{N}$-body probability distribution function by $\Psi_{\mathcal{N}}(\mathbf{r}_1, \hat{\mathbf{t}}_1, \cdots, \mathbf{r}_{\mathcal{N}}, \hat{\mathbf{t}}_{\mathcal{N}}, t)$. The distribution function is the probability of finding the αth swimmer at position $\mathbf{r}_\alpha$ with the orientation given by $\hat{\mathbf{t}}_\alpha$ at time t. This distribution function obeys the following normalization condition:

$$\prod_{\alpha=1}^{\mathcal{N}} \int \text{d}\mathbf{r}_\alpha \text{d}\hat{\mathbf{t}}_\alpha\, \Psi_{\mathcal{N}} = 1, \tag{30}$$

and it satisfies the following continuity equation:

$$\partial_t \Psi_{\mathcal{N}} = -\left(\sum_{\alpha=1}^{\mathcal{N}} \frac{\partial}{\partial \mathbf{r}_\alpha}\right) \cdot \mathbf{J}^{\text{T}}_{\mathcal{N}} - \left(\sum_{\alpha=1}^{\mathcal{N}} \hat{\mathbf{t}}_\alpha \times \frac{\partial}{\partial \hat{\mathbf{t}}_\alpha}\right) \cdot \mathbf{J}^{\text{R}}_{\mathcal{N}}, \tag{31}$$

where $\mathbf{J}^{\text{T}}_{\mathcal{N}}$ and $\mathbf{J}^{\text{R}}_{\mathcal{N}}$ are the translational and rotational $\mathcal{N}$-body fluxes. At a very small volume fraction of swimmers, where the distance between swimmers is larger than their size, we can treat the system at the mean-field level. In this case the $\mathcal{N}$-body distribution function can be given in terms of a single-particle distribution function:

$$\Psi_{\mathcal{N}} = \psi\left(\mathbf{r}_1, \hat{\mathbf{t}}_1, t\right) \cdots \psi\left(\mathbf{r}_{\mathcal{N}}, \hat{\mathbf{t}}_{\mathcal{N}}, t\right). \tag{32}$$

Using this assumption, the single-particle distribution function, $\psi\left(\mathbf{r}, \hat{\mathbf{t}}, t\right)$, obeys the following Smoluchowski equation:

$$\partial_t \psi = -\boldsymbol{\nabla} \cdot \mathbf{J}^{\text{T}} - \boldsymbol{\nabla}_{\text{R}} \cdot \mathbf{J}^{\text{R}}, \tag{33}$$

J. Stat. Mech. (2018) 023201

where $\mathbf{J}^{\mathrm{T}}$ and $\mathbf{J}^{\mathrm{R}}$ are the translational and rotational one-body fluxes and are given by:

$$\mathbf{J}^{\mathrm{T}} = \left[v_0 \hat{\mathbf{t}} + \overline{\mathbf{V}}^{\mathrm{int}} \right] \psi - \mathbf{D} \cdot \boldsymbol{\nabla} \psi, \tag{34}$$

$$\mathbf{J}^{\mathrm{R}} = \overline{\boldsymbol{\Omega}}^{\mathrm{int}} \, \psi - D_{\mathrm{R}} \, \boldsymbol{\nabla}_{\mathrm{R}} \, \psi. \tag{35}$$

The mean-field translational and rotational velocities are denoted by $\overline{\mathbf{V}}^{\mathrm{int}}$ and $\overline{\boldsymbol{\Omega}}^{\mathrm{int}}$. These mean-field terms should be calculated by integrating over the positions and orientations of all the swimmers:

$$\overline{\mathbf{V}}^{\mathrm{int}} \left(\mathbf{r}, \hat{\mathbf{t}}, t \right) = \int \mathrm{d}\mathbf{r}' \mathrm{d}\hat{\mathbf{t}}' \, \mathbf{V}^{\mathrm{int}}(\mathbf{r}, \mathbf{r}', \hat{\mathbf{t}}, \hat{\mathbf{t}}') \, \psi(\mathbf{r}', \hat{\mathbf{t}}', t), \tag{36}$$

$$\overline{\boldsymbol{\Omega}}^{\mathrm{int}} \left(\mathbf{r}, \hat{\mathbf{t}}, t \right) = \int \mathrm{d}\mathbf{r}' \mathrm{d}\hat{\mathbf{t}}' \, \boldsymbol{\Omega}^{\mathrm{int}}(\mathbf{r}, \mathbf{r}', \hat{\mathbf{t}}, \hat{\mathbf{t}}') \, \psi(\mathbf{r}', \hat{\mathbf{t}}', t). \tag{37}$$

In order to study the dynamics of an active system composed of interacting particles, we proceed and consider the dynamics of the moments of the distribution function. The density field $\rho(\mathbf{r}, t)$, polarization $\mathbf{P}(\mathbf{r}, t)$ and nematic-order parameter $\mathbf{N}(\mathbf{r}, t)$ are the first three moments of the distribution function, which are defined as follows:

$$\rho(\mathbf{r}, t) = \int \mathrm{d}\hat{\mathbf{t}} \, \psi(\mathbf{r}, \hat{\mathbf{t}}, t), \tag{38}$$

$$\rho(\mathbf{r}, t) \mathbf{P}(\mathbf{r}, t) = \int \mathrm{d}\hat{\mathbf{t}} \, \hat{\mathbf{t}} \, \psi(\mathbf{r}, \hat{\mathbf{t}}, t), \tag{39}$$

$$\rho(\mathbf{r}, t) \mathbf{N}(\mathbf{r}, t) = \int \mathrm{d}\hat{\mathbf{t}} \, \left(\hat{\mathbf{t}}\hat{\mathbf{t}} - \frac{\mathbf{I}}{3} \right) \psi(\mathbf{r}, \hat{\mathbf{t}}, t). \tag{40}$$

Using equation (33), we can obtain the equations that govern the dynamics of the above continuum fields. These equations show that the dynamics of the nth moment is coupled to the dynamics of the $(n-1)$th moment. So we need to cut the hierarchy at some point. As an approximation, we neglect the third (and higher) moment and cut the equations at the second moment. In this case and in terms of density, polarization and nematic order, the distribution function can be constructed as:

$$\psi(\mathbf{r}, \hat{\mathbf{t}}, t) = \rho(\mathbf{r}, t) \left(\frac{1}{4\pi} + \frac{3}{4\pi} \, \hat{\mathbf{t}} \cdot \mathbf{P}(\mathbf{r}, t) + \frac{15}{8\pi} \left(\hat{\mathbf{t}}\hat{\mathbf{t}} - \frac{\mathbf{I}}{3} \right) : \mathbf{N}(\mathbf{r}, t) \right). \tag{41}$$

3.3. Mean-field interactions

Before deriving the dynamical equations for continuum fields, we need to calculate the mean-field form of the interaction terms. As discussed before, the interaction between swimmers has two contributions, short- and long-range parts:

$$\begin{aligned} \overline{\mathbf{V}}^{\mathrm{int}} \left(\mathbf{r}, \hat{\mathbf{t}}, t \right) &= \overline{\mathbf{V}}^{\mathrm{S}} + \overline{\mathbf{V}}^{\mathrm{L}} \\ \overline{\boldsymbol{\Omega}}^{\mathrm{int}} \left(\mathbf{r}, \hat{\mathbf{t}}, t \right) &= \overline{\boldsymbol{\Omega}}^{\mathrm{S}} + \overline{\boldsymbol{\Omega}}^{\mathrm{L}}. \end{aligned} \tag{42}$$

J. Stat. Mech. (2018) 023201

To obtain the short-range contribution we need to insert the two-body interactions from equations (18) and (19) into equations (36) and (37) and then calculate the integrations. To obtain the final results, the following integral should be obtained:

$$\overline{\mathrm{U}}^{\mathrm{S}}(\mathbf{r},\hat{\mathbf{t}},t)=\int \mathrm{d}\mathbf{r}'\mathrm{d}\hat{\mathbf{t}}'\,\mathrm{U}^{\mathrm{S}}\,\psi(\mathbf{r}',\hat{\mathbf{t}}',t). \tag{43}$$

Now, as the interaction is short-range, we can expand $\psi(\mathbf{r}',\hat{\mathbf{t}}',t)$ as:

$$\psi(\mathbf{r}',\hat{\mathbf{t}}',t)=\psi(\mathbf{r},\hat{\mathbf{t}}',t)+(\mathbf{r}'-\mathbf{r})\cdot\partial_{\mathbf{r}}\psi(\mathbf{r},\hat{\mathbf{t}}',t)+\cdots. \tag{44}$$

The leading-order terms read as:

$$\overline{\mathrm{U}}^{\mathrm{S}}(\mathbf{r},\hat{\mathbf{t}},t)=-\frac{4}{3}\pi\ell_{\mathrm{c}}^{3}U_{0}k_{\mathrm{B}}T\left(1+\frac{1}{10}\ell_{\mathrm{c}}^{2}\,\nabla^{2}+\cdots\right)(\rho\,\hat{\mathbf{t}}\cdot\mathbf{P}). \tag{45}$$

Now the short-range contributions read as:

$$\begin{aligned}\overline{\mathbf{V}}^{\mathrm{S}}(\mathbf{r},\hat{\mathbf{t}},t)&=\frac{4}{3}\pi\ell_{\mathrm{c}}^{3}U_{0}\,\mathbf{D}\cdot\boldsymbol{\nabla}\left(\rho\,\hat{\mathbf{t}}\cdot\mathbf{P}\right)+\cdots,\\ \overline{\boldsymbol{\Omega}}^{\mathrm{S}}(\mathbf{r},\hat{\mathbf{t}},t)&=\frac{4}{3}\pi\ell_{\mathrm{c}}^{3}U_{0}\,D_{\mathrm{R}}\boldsymbol{\nabla}_{\mathrm{R}}\left(\rho\,\hat{\mathbf{t}}\cdot\mathbf{P}\right)+\cdots.\end{aligned} \tag{46}$$

Long-range contributions can also be obtained by inserting (7) and (8) into equations (36) and (37). In terms of their components, the mean-field long-range interactions can be written as:

$$\overline{V}_{i}^{\mathrm{L}}(\mathbf{r},\hat{\mathbf{t}},t)=b_{1}T_{i}^{1}(\mathbf{r},t)+b_{2}T_{i}^{2}(\mathbf{r},t)+b_{3}T_{il}^{3}(\mathbf{r},t)\,\hat{t}_{l}, \tag{47}$$

$$\overline{\Omega}_{i}^{\mathrm{L}}(\mathbf{r},\hat{\mathbf{t}},t)=b_{1}T_{il}^{4}(\mathbf{r},t)\,\hat{t}_{l}-b_{2}T_{il}^{5}(\mathbf{r},t)\,\hat{t}_{l}+b_{4}T_{ilm}^{6}(\mathbf{r},t)\,\hat{t}_{l}\hat{t}_{m}, \tag{48}$$

where summation over repeated indices is assumed and the coefficients are given by:

$$\begin{aligned}&b_{1}=\frac{261}{56}\,a\,\ell\,v_{0}\,\delta,\qquad b_{2}=-\frac{18}{35}\,\ell^{3}\,v_{0}\,(2+\delta)\,,\qquad b_{3}=\frac{5}{2}\,b_{2},\\ &b_{4}=-\frac{45}{4}\ell^{3}\,v_{0}\,(2-\delta)\,.\end{aligned} \tag{49}$$

To keep track of the singularities in equations (7) and (8), note that the terms proportional to b_1, b_2 and b_3 correspond to the terms proportional to a_1, a_2 and a_3 or equivalently all $\mathbf{T}^{\alpha}$ correspond to the $\mathbf{G}_{\alpha}$ defined before. Functions $\mathbf{T}^{1},\cdots,\mathbf{T}^{6}$ in (47) and (48) are functions of position and their detailed structures are given by:

$$T_{i}^{1}(\mathbf{r},t)=\int \mathrm{d}\mathbf{r}'\,\frac{\hat{R}_{i}}{R^{2}}\,M_{jk}(\hat{\mathbf{R}})\,\rho(\mathbf{r}',t)\,N_{jk}(\mathbf{r}',t), \tag{50}$$

$$T_{i}^{2}(\mathbf{r},t)=\int \mathrm{d}\mathbf{r}'\,\frac{1}{R^{3}}\,M_{ij}(\hat{\mathbf{R}})\,\rho(\mathbf{r}',t)\,P_{j}(\mathbf{r}',t), \tag{51}$$

$$T_{il}^{3}(\mathbf{r},t)=\int \mathrm{d}\mathbf{r}'\,\partial_{l}\left(\frac{M_{jk}(\hat{\mathbf{R}})}{R^{3}}\,R_{i}\right)\rho(\mathbf{r}',t)\,N_{jk}(\mathbf{r}',t), \tag{52}$$

J. Stat. Mech. (2018) 023201

$$T^4_{il}(\mathbf{r},t) = \int \mathrm{d}\mathbf{r}' \, \frac{\hat{R}_i}{R^3} \, M_{jkl}(\hat{\mathbf{R}}) \, \rho(\mathbf{r}',t) \, N_{jk}(\mathbf{r}',t), \tag{53}$$

$$T^5_{il}(\mathbf{r},t) = \int \mathrm{d}\mathbf{r}' \, \frac{1}{R^4} \, M_{ijl}(\hat{\mathbf{R}}) \, \rho(\mathbf{r}',t) \, P_j(\mathbf{r}',t), \tag{54}$$

$$T^6_{ilm}(\mathbf{r},t) = \int \mathrm{d}\mathbf{r}' \, \frac{\hat{R}_i}{R^4} \, M_{jklm}(\hat{\mathbf{R}}) \, \rho(\mathbf{r}',t) \, N_{jk}(\mathbf{r}',t). \tag{55}$$

Taking a look at the mean-field velocities (47) and (48), we can see that long-range hydrodynamic interactions have a nematic nature. Regarding the discussion about singularities, the most important term that appears in the interactions is a term proportional to a_1 or equivalently b_1, which is the field due to a force dipole and is proportional to $\mathbf{T}^1$. Results show a nonlocal dependence on the nematic tensor N_{jk}. We will see in the following sections that terms with coefficient b_1, which are related to the nematic part of hydrodynamic interactions, have a significant impact on the long-wavelength behavior of the suspension.

In the next sections, we use the above results and study the dynamics of a suspension in the continuum limit.

4. Continuum description

Now we can calculate the dynamical equations for the hydrodynamic continuum fields. Starting from equation (33), multiplying both sides by powers of $\hat{\mathbf{t}}$ and integrating over a solid angle spanned by $\hat{\mathbf{t}}$, we can obtain the equations that govern the dynamics of the density, polarization and nematic-order parameter. The results of such calculations can be written as:

$$\partial_t \rho = -v_0 \boldsymbol{\nabla}.(\rho \mathbf{P}) + D_1 \nabla^2 \rho + D_2 \, \partial_i \partial_j (\rho N_{ij}) + \dot{\rho}^{\mathrm{L}} + \dot{\rho}^{\mathrm{S}}, \tag{56}$$

$$\begin{aligned} \partial_t (\rho P_i) = &- v_0 \partial_j \left(\rho N_{ij}\right) - \frac{1}{3} v_0 \partial_i \rho - 2 D_{\mathrm{R}} \rho P_i \\ &+ \partial_j \left(\frac{2}{5} D_2 \, \partial_i (\rho P_j) + D_3 \partial_j \left(\rho P_i\right) \right) + \dot{P}^{\mathrm{L}}_i + \dot{P}^{\mathrm{S}}_i, \end{aligned} \tag{57}$$

$$\begin{aligned} \partial_t (\rho N_{ij}) = &- \frac{1}{5} v_0 \left[\partial_i (\rho P_j) + \partial_j (\rho P_i)\right] + \frac{2}{15} v_0 \, \delta_{ij} \boldsymbol{\nabla} \cdot (\rho \mathbf{P}) \\ &- 6 D_{\mathrm{R}} \rho N_{ij} + \frac{2}{15} D_2 \left(\partial_i \partial_j - \frac{1}{3} \delta_{ij} \nabla^2 \right) \rho \\ &+ \frac{2}{7} D_2 \partial_k \left(\partial_i (\rho N_{jk}) + \partial_j (\rho N_{ik}) - \frac{2}{3} \delta_{ij} \partial_l (\rho N_{kl}) \right) \\ &+ D_4 \nabla^2 (\rho N_{ij}) + \dot{N}^{\mathrm{L}}_{ij} + \dot{N}^{\mathrm{S}}_{ij}. \end{aligned} \tag{58}$$

https://doi.org/10.1088/1742-5468/aaa795

J. Stat. Mech. (2018) 023201

As one can see, in addition to the diffusion and swimmer activity terms, the terms proportional to v_0, there are contributions from the interactions. Contributions from long-range and short-range interactions are collected in terms that are denoted by superscripts L and S respectively ($\dot{\rho}^{\mathrm{L}}$, $\dot{\rho}^{\mathrm{S}}$, etc). To keep the continuity of the text, we put these interaction terms in appendix C. The effective diffusion coefficients in the above equations are defined as:

$$D_1 = \frac{1}{3}\left(D_\parallel + 2D_\perp\right), \quad D_2 = D_\parallel - D_\perp,$$
$$D_3 = \frac{1}{5}\left(D_\parallel + 4D_\perp\right), \quad D_4 = \frac{1}{7}\left(D_\parallel + 6D_\perp\right). \tag{59}$$

Equation (56) shows the conservation of density. Convection along the intrinsic velocity is reflected by the first term; the second and third terms show diffusion along the density and nematic gradients. The first two terms in equation (57) show that the gradients in the density and nematic fields have contributions to the dynamics of polarization. Compared to the Navier–Stokes equation, these terms can be regarded as pressure gradients. The terms proportional to D_2 and D_3 in equation (57) with similar counterparts in Toner and Tu's description [20] are diffusion terms. The term $-2D_{\mathrm{R}}\rho P_i$ together with the last term in the short-range part of this equation ($\dot{P}_i^{\mathrm{S}}$) is responsible for developing a homogeneous polar phase in our system. Such terms have counterparts in phenomenologically derived continuum equations [2, 20, 45].

4.1. Steady-state solutions

Here we seek steady-state uniform solutions to the above dynamical equations for continuum fields. Terms corresponding to long-range interactions and the swimmer's activity do not contribute to uniform steady-state solutions. Steady states are solutions to the following equations:

$$\partial_t \rho = 0, \tag{60}$$

$$\partial_t(\rho P_i) = -2D_{\mathrm{R}}\rho P_i + \frac{4}{3}\pi D_{\mathrm{R}}\ell_{\mathrm{c}}^3 U_0 \rho^2 \left(\frac{2}{3}P_i - P_j N_{ij}\right), \tag{61}$$

$$\partial_t(\rho N_{ij}) = -6D_{\mathrm{R}}\rho N_{ij} + \frac{8}{5}\pi D_{\mathrm{R}}\ell_{\mathrm{c}}^3 U_0 \rho^2 \left(P_i P_j - \frac{P^2}{3}\delta_{ij}\right). \tag{62}$$

The above equations show that there are two different homogeneous steady-state phases in our system. The first phase, denoted by I, is an isotropic phase and is defined by:

$$\rho^{\mathrm{I}} = \rho_0, \quad \mathbf{P}^{\mathrm{I}} = 0 \quad \mathbf{N}^{\mathrm{I}} = 0. \tag{63}$$

In this phase, all swimmers are distributed uniformly in the fluid and move randomly without any preferred direction. Increasing the density, we see that beyond a critical density $\rho_0 > \rho_{\mathrm{c}} = 9/(4\pi\ell_{\mathrm{c}}^3 U_0)$, a homogeneous polarized state appears. This phase is denoted by P and defined by:

$$\rho^{\mathrm{P}} = \rho_0, \quad \mathbf{P}^{\mathrm{P}} = \mathbf{P}^{\infty}, \quad \mathbf{N}^{\mathrm{P}} = \mathbf{N}^{\infty}. \tag{64}$$

J. Stat. Mech. (2018) 023201

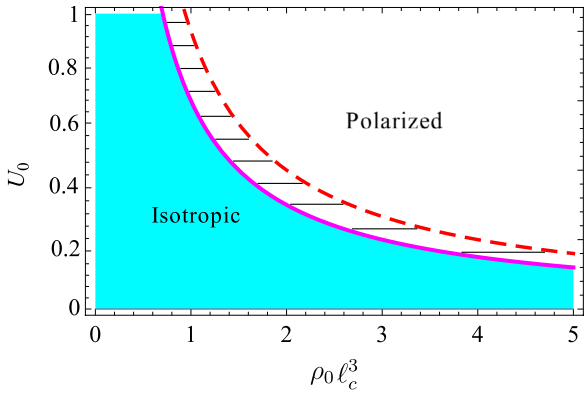

Figure 3. Phase diagram showing possible thermodynamic phases for a suspension of swimmers. Isotropic and polarized phases are separated by a solid line in a space given by U_0 (strength of short-range interaction) and $\rho_0\ell_c^3$ (density of swimmers). Taking into account long-wavelength fluctuations, calculations show that both phases are unstable. Part of the polarized phase denoted by dashed lines shows the states that are stable with respect to splay fluctuations. These states are unstable with respect to bend fluctuations.

In this polarized phase, swimmers are distributed uniformly and move in a preferred direction. Steady-state polarization and the nematic-order parameter in the polar phase are given by:

$$\mathbf{P}^{\infty} = \sqrt{\frac{15}{4\pi\ell_c^3\rho_0 U_0}\left(1 - \frac{9}{4\pi\ell_c^3\rho_0 U_0}\right)}\,\hat{\mathbf{n}}, \tag{65}$$

$$\mathbf{N}^{\infty} = \left(1 - \frac{9}{4\pi\ell_c^3\rho_0 U_0}\right)\left(\hat{\mathbf{n}}\hat{\mathbf{n}} - \frac{\mathbf{I}}{3}\right), \tag{66}$$

where $\hat{\mathbf{n}}$ denotes the direction of the broken symmetry. Figure 3 shows a phase diagram in a space characterized by U_0 and $\rho_0\ell_c^3$. Appearance of the ordered phase is a direct consequence of the short-range (alignment) interaction between the swimmers. As is apparent from the equations, long-range interactions alone are not able to induce any ordered state in bulk [32]. It has been shown very recently that short-range hydrodynamic interactions in symmetric squirmers are also able to induce a polar state [60].

4.2. Stability of isotropic state

In addition to the existence of steady-state phases, their stability is important to analyze. Thermal or non-thermal fluctuations can destabilize the above steady-state phases. In this section, we study the stability of the steady-state solutions.

To study the stability of the isotropic phase, we add small fluctuations to the corresponding fields of the isotropic state and investigate their dynamics:

$$\rho(\mathbf{r}, t) = \rho_0 + \delta\rho(\mathbf{r}, t), \tag{67}$$

$$\mathbf{P}(\mathbf{r}, t) = 0 + \delta\mathbf{P}(\mathbf{r}, t), \tag{68}$$

J. Stat. Mech. (2018) 023201

$$\mathbf{N}(\mathbf{r},t) = 0 + \delta\mathbf{N}(\mathbf{r},t). \tag{69}$$

Using the dynamical equations obtained in the above section, we can obtain the evolution equations of these fluctuating fields. To linearize the equations, we introduce spatial Fourier transformation:

$$\check{f}(\mathbf{k}) = \int \mathrm{d}\mathbf{r}\, \mathrm{e}^{\mathrm{i}\mathbf{k}\cdot\mathbf{r}}\, f(\mathbf{r}). \tag{70}$$

In appendix C, we show how a typical term in the dynamical equation can be linearized. Repeating the same procedure for all other terms, we can arrive at the following equations that describe the linearized dynamics of the fluctuations around the isotropic phase:

$$\partial_t \delta\check{\rho} = \mathrm{i}v_0\rho_0 k_i \delta\check{P}_i - \frac{8\pi\mathrm{i}}{9} b_2 \rho_0^2 k_i \delta\check{P}_i - D_1 k^2 \delta\check{\rho} - \rho_0 D_2 k_i k_j \delta\check{N}_{ij}, \tag{71}$$

$$\begin{aligned}\partial_t \delta\check{P}_i =& \mathrm{i}v_0 k_j \delta\check{N}_{ij} + \mathrm{i}\frac{v_0}{3\rho_0}\delta\check{\rho}k_i - \frac{8\pi\mathrm{i}}{45} b_3 \rho_0 k_j \delta\check{N}_{ij} - \frac{2}{5} D_2 k_j \delta\check{P}_j k_i - D_3 k^2 \delta\check{P}_i \\ &+ \frac{4}{9}\pi\ell_\mathrm{c}^3 U_0 \rho_0 \left(\frac{1}{5} D_2 [2k_j\delta\check{P}_j k_i + k^2 \delta\check{P}_i] + D_\perp k^2 \delta\check{P}_i\right) - 2D_\mathrm{R}\delta\check{P}_i \\ &+ \frac{8}{9}\pi D_\mathrm{R}\ell_\mathrm{c}^3 U_0\rho_0\delta\check{P}_i - \frac{32\pi\mathrm{i}}{225} b_4\rho_0 k \left(-\hat{k}_j\hat{k}_k\delta\check{N}_{jk}\hat{k}_i + \frac{14}{35}\delta\check{N}_{ik}\hat{k}_k\right)\end{aligned} \tag{72}$$

and

$$\begin{aligned}\partial_t \delta\check{N}_{ij} =& \frac{2}{5}\mathrm{i}v_0\left(\frac{1}{2}[k_i\delta\check{P}_j + k_j\delta\check{P}_i] - \frac{1}{3}k_k\delta\check{P}_k\delta_{ij}\right) - \frac{2}{15\rho_0} D_2 k_i k_j \delta\check{\rho} \\ &+ \frac{2}{45} D_2 k^2 \delta_{ij}\frac{\delta\check{\rho}}{\rho_0} - 6D_R\delta\check{N}_{ij} - D_4 k^2 \delta\check{N}_{ij} - \frac{2}{7} D_2 \Bigg(k_z k_i \delta\check{N}_{jz} \\ &+ k_z k_j \delta\check{N}_{iz} - \frac{2}{3}\delta_{ij}k_k k_l \delta\check{N}_{kl}\Bigg) + \frac{\rho_0}{5}\Bigg(\frac{8\pi}{3} b_1 [2\hat{k}_k\hat{k}_l\delta\check{N}_{kl}\hat{k}_i\hat{k}_j \\ &- \delta\check{N}_{ik}\hat{k}_k\hat{k}_j - \delta\check{N}_{jk}\hat{k}_k\hat{k}_i + \frac{2}{5}\delta\check{N}_{ij}] + \frac{8\pi\mathrm{i}}{15} b_2 [5k_k\delta\check{P}_k\hat{k}_i\hat{k}_j \\ &- \delta\check{P}_i k_j - \delta\check{P}_j k_i - k_k\delta\check{P}_k\delta_{ij}]\Bigg).\end{aligned} \tag{73}$$

These coupled equations govern the dynamics of fluctuations. As one can distinguish from these equations, convection (terms proportional to v_0), diffusion (terms proportional to D_i), short-range interactions (terms proportional to U_0) and long-range interactions (terms proportional to b_i) have contributions to the dynamics.

It should be mentioned that in order to investigate the stability of the isotropic phase, we have to consider the nematic order as well as the polar order. This is a direct result of the nature of hydrodynamic interaction we derived before. According to equations (47) and (48) and their discussion above, the most important part of the interactions directly takes into account the nematic order. In the absence of such a term in

J. Stat. Mech. (2018) 023201

the hydrodynamic interaction, the nematic order is subjugated to the polar order and it is an irrelevant field [46]. According to the above equation, the strongest contribution from hydrodynamic interactions appears only in nematic fluctuations (equation (73)) and it is a term that is proportional to b_1. As analysis of the above coupled equations is not simple, we can use different approximations to understand the physical mechanisms of possible instabilities.

As a first approximation that is at times longer than the time scale of rotational diffusion ($t \gg D_{\mathrm{R}}^{-1}$), we can neglect the dynamics of $\delta\check{P}_i$ and $\delta\check{N}_{ij}$ in equations (72) and (73). Solving the simplified equations for polarization and nematic fluctuations ($\partial_t\delta\check{P}_i = \partial_t\delta\check{N}_{ij} \to 0$), we can substitute them in equation (71) and keep the leading-order powers of wave vector k. This results in an effective diffusion equation for density fluctuations:

$$\partial_t\delta\check{\rho} = -D_{\mathrm{eff}}k^2\delta\check{\rho}, \tag{74}$$

where the effective diffusion constant is given by:

$$D_{\mathrm{eff}} = D_1 + \frac{v_0^2}{D_{\mathrm{R}}(3 - \frac{4}{3}\pi\ell_{\mathrm{c}}^3\rho_0 U_0)}\left[\frac{1}{2} + \frac{8\pi\rho_0\ell^3}{35}\right]. \tag{75}$$

Since in the isotropic phase $\ell_{\mathrm{c}}^3\rho_0 U_0 < 9/4\pi$, the above effective diffusion coefficient is always positive and it is greater than the diffusion coefficient of a Brownian self-propelled rod, $D_1 + v_0^2/6D_{\mathrm{R}}$ [61]. As a result of the positivity of D_{eff}, density fluctuations are damped and the isotropic state is stable if we neglect polarization and nematic fluctuations.

It is a well-known fact that for an active Brownian particle, orientational fluctuations increase the translational diffusion by a term proportional to v_0^2/D_{R}, but what is new here is the effect of hydrodynamic interactions. In the above result, the second term in brackets, $(8\pi/35)\rho_0\ell^3$, which is due to hydrodynamic interaction, shows that the hydrodynamic interaction speeds up the diffusion process. The increase in diffusion due to the hydrodynamic interaction is proportional to the density of swimmers and to the size of an individual swimmer.

To have more insights into fluctuations in the isotropic phase, we study the dispersion relation for hydrodynamic modes in the system. In this case, we do not base our approximation on neglecting the dynamics of polarization and the nematic-order parameter from the above coupled equations. It is apparent from equations (72) and (73) that the nematic fluctuations are coupled to the density fluctuations in higher powers of the wave vector. We are interested in long-wavelength fluctuations, so as another approximation we may discard nematic fluctuations ($\delta\check{N}_{ij} \to 0$) and consider only the coupled dynamics of density and polarization fluctuations. Assuming a time-dependent form for the fluctuations,

$$\delta\check{\rho}, \delta\check{P}_i \sim \mathrm{e}^{\chi(k)\,t}, \tag{76}$$

we can study their coupled dynamics and obtain a dispersion relation like $\chi = \chi(k)$. Up to the leading orders of k, the dispersion relation reads:

J. Stat. Mech. (2018) 023201

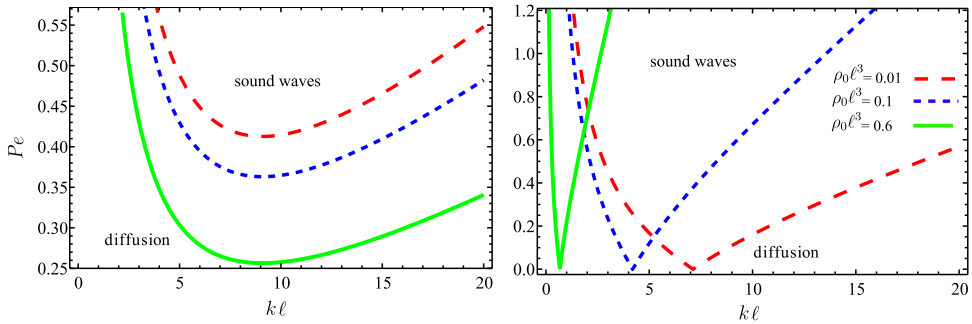

Figure 4. For a system with given $\rho_0\ell^3$ and depending on the value of the Péclet number $\mathrm{Pe} = \frac{v_0\,\ell}{D_\parallel}$, a fluctuating mode with wave vector $k\ell$ can propagate with a diffusion or sound wave mechanism. Lines show the boundary between these two different behaviors. The left graph is for a system that has only long-range interactions and the right graph shows the results for a system that has both short- and long-range interactions. The numerical values we use are $\delta = 0.1$, $a/\ell = 0.1$, $\ell_c/\ell = 1$ and $U_0 = 1$.

$$\chi_\pm = \frac{1}{54}\Bigg[-9\left(3 - \frac{4}{3}\pi\ell_c^3\rho_0 U_0\right)(2D_R + D_5k^2) - 27D_1k^2 \pm \Bigg[\left(9\left(3 - \frac{4}{3}\pi\ell_c^3\rho_0 U_0\right)(2D_R + D_5k^2) + 27D_1k^2\right)^2 + 108\Bigg(-9D_1k^2\left(3 - \frac{4}{3}\pi\ell_c^3\rho_0 U_0\right)(2D_R + D_5k^2) - 9v_0^2k^2\left(1 + \frac{16\pi}{35}\rho_0\ell^3(2+\delta)\right)\Bigg)\Bigg]^{1/2}\Bigg], \tag{77}$$

where $D_5 = 1/5\,(3D_\parallel + 2D_\perp)$. As we expected from the previous discussion, for $\ell_c^3\rho_0 U_0 < 9/4\pi$, both χ_+ and χ_- are negative, reflecting the fact that the isotropic phase is always stable. It should also be noted that although the two modes always have negative real values, if the self-propulsion speed of the swimmers is greater than a threshold value, they will have an imaginary part. As a result of this imaginary part, fluctuations of density and polarization decay with a propagating mechanism and propagating sound waves appear in the system [62]. In terms of the Péclet number $\mathrm{Pe} = (v_0\,\ell)/D_\parallel$ and the dimensionless wave vector $k\ell$, figure 4 shows the regions where these waves can propagate. For an intermediate $k\ell$, density waves appear at larger Pe. As seen in figure 4 (left), taking into account only the long-range part of the interactions, increasing the density decreases the threshold Pe above which propagating waves appear. Taking into account both long- and short-range interactions in figure 4 (right), we see that lower densities of swimmers have a wider region for density waves. Interestingly, all these results are valid for both pushers and pullers.

The above approximations show that density and polarization fluctuations are not able to induce any instability in the isotropic phase. To see how nematic fluctuations can provide a mechanism for instability, we can study their dynamics separately.

J. Stat. Mech. (2018) 023201

Arranging the right-hand side of equation (73) in powers of k, we can study the nematic fluctuations at the long-wavelength limit. Keeping the leading-order term, we find that the nematic fluctuations are decoupled from the density and polarization:

$$\partial_t \delta N_{\rm s} = \left(-6D_{\rm R} + \frac{16\pi}{75}\rho_0 b_1\right)\delta N_{\rm s}, \tag{78}$$

$$\partial_t \delta \mathbf{N}_{\rm b} = \left(-6D_{\rm R} - \frac{8\pi}{25}\rho_0 b_1\right)\delta \mathbf{N}_{\rm b}, \tag{79}$$

where the nematic fluctuations are decomposed into their splay component $\delta N_{\rm s} = \hat{\mathbf{k}}\cdot\delta\check{\mathbf{N}}\cdot\hat{\mathbf{k}}$ and bend component $\delta\mathbf{N}_{\rm b} = \hat{\mathbf{k}}\cdot\delta\check{\mathbf{N}}\cdot\left(\mathbf{I}-\hat{\mathbf{k}}\hat{\mathbf{k}}\right)$. Coefficient b_1 is proportional to the asymmetry parameter δ and for pullers (pushers) it is positive (negative). This shows that if the density of swimmers is greater than the value given by $\rho_{\rm ins} \propto D_{\rm R}/|b_1|$, splay (bend) perturbations in the nematic tensor can destabilize an isotropic suspension of pullers (pushers). As we discuss above, instability in a suspension of both pullers and pushers is due to the nematic part of hydrodynamic interactions. It should be mentioned that instabilities of the isotropic phase have been reported before [21, 27, 32, 34]. In [32] instability of an isotropic suspension of pullers and pushers was observed. Comparison with our results shows that for the case of pushers our results are in agreement but for pullers the growth of fluctuations in [32] has a diffusive nature and is non-compatible with our results. In other works [21, 27, 34], it has been shown by employing a kinetic model that an isotropic suspension of pushers is always unstable but no instability is seen for pullers. The instability observed in these works is for non-spherically symmetric particles. We should emphasize that we agree with this result in the sense that our swimmer is also hydrodynamically anisotropic (even at the limit $D_\perp = D_\parallel$). So the instabilities that we observe in the current work are valid for anisotropic particles.

4.3. Stability of polar state

To study the stability of the polar phase, we assume that the density of swimmers is higher than $\rho_{\rm c}$, so that the polarized phase is established. Then we study the dynamics of fluctuations around the polarized state. Denoting by $\hat{\mathbf{n}}$ the direction of polarization, we suppose that the order parameter has a constant value but its direction fluctuates. In this case, hydrodynamic fields can be written as:

$$\rho = \rho_0 + \delta\rho, \tag{80}$$

$$\mathbf{P} = P^\infty\left(\hat{\mathbf{n}}_0 + \delta\mathbf{n}\right), \tag{81}$$

$$\mathbf{N} = N^\infty\left((\hat{\mathbf{n}}_0 + \delta\mathbf{n})(\hat{\mathbf{n}}_0 + \delta\mathbf{n}) - \frac{\mathbf{I}}{3}\right), \tag{82}$$

where we assume $\hat{\mathbf{n}} = \hat{\mathbf{n}}_0 + \delta\mathbf{n}$, with $\hat{\mathbf{n}}_0$ denoting the average direction of polarization in the system. Furthermore, for small fluctuations we have $\hat{\mathbf{n}}_0\cdot\delta\mathbf{n} = 0$. Using the above definitions, we can linearize equations (56) and (57) and obtain evolution equations for

J. Stat. Mech. (2018) 023201

density and director fluctuations. Since we are making our calculations in the Fourier space, the angle between the wave vector $\mathbf{k}$ and director $\hat{\mathbf{n}}_0$ will emerge in the linearized equations. To simplify the analysis, we decompose the fluctuations into bend and splay distortions. A splay distortion is a fluctuation with $\nabla \cdot \mathbf{P} \neq 0$ ($\nabla \cdot \delta\mathbf{n} \neq 0$) and for bend fluctuations $\mathbf{P} \times (\nabla \times \mathbf{P}) \neq 0$ ($\nabla \times \delta\mathbf{n} \neq 0$). Decomposing the wave vector $\mathbf{k}$ into its parallel and perpendicular components, $\mathbf{k} = (\mathbf{k} \cdot \hat{\mathbf{n}}_0)\hat{\mathbf{n}}_0 + \mathbf{k}_\perp$, we can see that for bend (splay) fluctuations only the parallel (perpendicular) component of the wave vector contributes. These two modes of fluctuations are independent and this allows us to study them separately.

To study the bend fluctuations, we can set $\mathbf{k} = k\hat{\mathbf{n}}_0$ and study the dynamics of the fluctuations. Using a linearization procedure similar to what we use in the previous section and keeping terms up to the second order of the wave vector, we can arrive at the following equations for bend fluctuations:

$$\partial_t \delta\check{\rho}_\mathrm{b} = \left(\mathrm{i}\,\chi_\rho^{\mathrm{Im}} + \chi_\rho^{\mathrm{Re}}\right)\delta\check{\rho}_\mathrm{b}, \tag{83}$$

$$\partial_t \delta\check{\mathbf{n}}_\mathrm{b} = \left(\mathrm{i}\,\chi_n^{\mathrm{Im}} + \chi_n^{\mathrm{Re}}\right)\delta\check{\mathbf{n}}_\mathrm{b}, \tag{84}$$

where the imaginary and real parts are given by:

$$\chi_\rho^{\mathrm{Re}} = -\frac{16\pi}{9}\rho_0\, N^\infty\, b_1 + k^2\left(-D_1 + N^\infty\, D_6\right), \tag{85}$$

$$\chi_\rho^{\mathrm{Im}} = P^\infty\, k\left(v_0 - \frac{8\pi}{9}\rho_0\, b_2 + \frac{64\pi}{45}\rho_0\, N^\infty\, b_3\right), \tag{86}$$

$$\chi_n^{\mathrm{Re}} = -\frac{136\pi}{75}b_1\rho_0 N^\infty + \frac{4}{35}k^2\, D_2\left(\frac{4}{3}\pi\ell_\mathrm{c}^3\rho_0 U_0 - 3\right), \tag{87}$$

$$\begin{aligned}\chi_n^{\mathrm{Im}} = \frac{k}{\rho_0 P^\infty}\Bigg(& v_0\rho_0 N^\infty - \frac{8\pi}{45}\rho_0^2 b_3 N^\infty(1-N^\infty) \\ & - \frac{4\pi}{25}b_2\rho_0^2 P^{\infty 2} - b_4\rho_0^2 N^\infty\left[\frac{2368}{(105)^2}N^\infty + \frac{192}{875}\right]\Bigg),\end{aligned} \tag{88}$$

with $D_6 = 1/3\,(7D_\parallel + 8D_\perp)$. As seen from the above equations, fluctuations of density and polarization are decoupled for the case of bend distortions. Both modes show that sound-like density waves can propagate in the system—regions with a dense-ordered population of particles propagating in a disordered background. The propagation of these waves is a signature of Vicsek-type flocking models [16, 40].

To analyze the stability of the polar state against bend fluctuations, let us consider two cases: one without hydrodynamic interactions and one with hydrodynamic interactions. The terms proportional to b_i in the above equations originate from long-range hydrodynamic interactions. In the absence of hydrodynamic interactions where $b_i = 0$, the real parts in both of the above equations are of order k^2, revealing the diffusing nature of the fluctuations. Moreover, under these conditions density fluctuations are damped for $\ell_\mathrm{c}^3\rho_0 U_0 < \frac{3}{4\pi}\frac{7D_\parallel + 8D_\perp}{2(D_\parallel + D_\perp)} \sim 0.9$ (we use the following numerical values: $\delta = 0.1$

J. Stat. Mech. (2018) 023201

and $a/\ell = 0.1$). These states are denoted by the dashed region in figure 3. Beyond this region and for $\ell_c^3\rho_0 U_0 > 0.9$, density fluctuations can grow and form clusters of swimmers. Considering the polarization fluctuations, we can see that for $\ell_c^3\rho_0 U_0 > 9/4\pi$, such fluctuations can always grow and make the polar state unstable.

Taking into account both short- and long-range interactions and in the limit of long-wavelength fluctuations ($k \to 0$), the terms that are proportional to b_1 in (85) and (87) are the most important terms that determine the instability criterion. Recalling the fact that $b_1 \propto \delta$, we see that for pullers ($\delta > 0$) density and director fluctuations diminish, but they diverge for pushers ($\delta < 0$). The growth of bend fluctuations destabilizes any polar order in a suspension of pushers [44].

To study the role of splay fluctuations, we set $\mathbf{k} = \mathbf{k}_\perp = k\hat{\mathbf{n}}_\perp$, with $\hat{\mathbf{n}}_\perp \cdot \hat{\mathbf{n}}_0 = 0$. For splay distortions, fluctuations of density and the director are always coupled to each other and they obey the following equations:

$$\partial_t \delta\check{\rho}_s = H_{11}\delta\check{\rho}_s + H_{12}\,\delta\check{n}_s, \tag{89}$$

$$\partial_t \delta\check{n}_s = H_{21}\delta\check{\rho}_s + H_{22}\,\delta\check{n}_s, \tag{90}$$

where

$$H_{11} = \frac{8}{9}\pi b_1\rho_0 N^\infty + k^2\left(-D_1 + N^\infty D_7\right), \tag{91}$$

$$H_{12} = \mathrm{i}k\rho_0 P^\infty\left(v_0\mathrm{i} - \frac{8}{9}\pi b_2\rho_0 - \frac{2}{5}\pi b_3\rho_0 N^\infty\right), \tag{92}$$

$$\begin{aligned} H_{21} = \frac{\mathrm{i}k}{\rho_0 P^\infty}\Bigg(&\frac{1}{3}v_0(1-N^\infty) + \frac{32\pi}{135}\rho_0 b_3 N^\infty\left(\frac{2}{7}N^\infty - 1\right) \\ &- \frac{4\pi}{25}\rho_0 b_2 P^{\infty 2} - \frac{16\pi}{175}\rho_0 b_4 N^\infty\left(\frac{6}{5} + \frac{29}{63}N^\infty\right)\Bigg), \end{aligned} \tag{93}$$

$$H_{22} = \frac{64\pi}{75}b_1\rho_0 N^\infty - \frac{3}{35}D_2 k^2\left(\frac{4}{3}\pi\ell_c^3\rho_0 U_0 - 3\right), \tag{94}$$

with $D_7 = 1/3\,(4D_\parallel + 11D_\perp)$ and $\delta\check{n}_s = \hat{\mathbf{n}}_\perp \cdot \delta\check{\mathbf{n}}$. By calculating the eigenvalues of matrix $\mathbf{H}$, we obtain two dispersion relations for the fluctuation spectrum. In the absence of hydrodynamic interactions, the spectrum of fluctuations has a simpler form:

$$\chi_\pm = \pm\frac{\mathrm{i}kv_0}{\sqrt{\frac{4}{3}\pi\ell_c^3\rho_0 U_0}} + k^2\left(D_8 - \frac{3D_9}{4\pi\ell_c^3\rho_0 U_0} - \frac{2}{35}\pi\ell_c^3\rho_0 U_0 D_2\right), \tag{95}$$

where $D_8 = 2/35(11D_\parallel + 24D_\perp)$, $D_9 = 1/2(4D_\parallel + 11D_\perp)$. The real part of this relation is negative for $\ell_c^3\rho_0 U_0 < 0.9$, reflecting the fact that in the absence of hydrodynamic interactions, splay fluctuations decay to zero when $9/4\pi < \ell_c^3\rho_0 U_0 < 0.9$ (dashed region in figure 3). But for $\ell_c^3\rho_0 U_0 > 0.9$, above the red dashed line in figure 3, splay fluctuations diverge, hence making the polarized state unstable.

J. Stat. Mech. (2018) 023201

If we consider the contributions from hydrodynamic interactions in the long-wavelength limit, the dispersion relations for the splay fluctuations read as:

$$\chi_+ = \frac{4}{5}\pi\rho_0 N^\infty b_1 + \mathcal{O}(k)^2, \quad \chi_- = \frac{1}{5}\pi\rho_0 N^\infty b_1 + \mathcal{O}(k)^2. \tag{96}$$

As for bend fluctuations, the sign of $b_1 \propto \delta$ determines the criterion for instability. For a suspension of pullers ($b_1 > 0$) fluctuations grow but for pushers ($b_1 < 0$) fluctuations are damped to zero. So an ordered suspension of pullers becomes unstable because of the growth of splay fluctuations.

5. Summary and discussion

In this article, we start from a microscopic model for a hydrodynamic micro-swimmer and derive its average dynamical characteristics such as its velocity and force distribution. The swimmer that we start with is able to model both pushers and pullers. We show that a set of analytical expressions can be obtained for the long-range interactions between two swimmers. Extending the system to a three-dimensional dilute suspension of swimmers and considering two-body interaction between swimmers, we develop a continuum description that can capture long-wavelength properties of the suspension. Furthermore, we assume that in addition to long-range interactions, there is a short-range interaction that can align nearby swimmers.

The aim of this article is to investigate the role of interactions in long-wavelength instabilities of a suspension. An isotropic phase and a symmetry-broken polar phase are well-known phases for systems with only short-range alignment interactions [42]. At a low density of swimmers, the system is in isotropic phase and increasing the density changes the system to a polar phase. In a system with hydrodynamic interactions, both of the above phases are unstable with respect to long-wavelength fluctuations.

It is long-range interaction that initiates instability in an interacting suspension. Our results are compatible with the well-known results of phenomenological models that state the origin of instability. Decomposing nematic distortions into bend and splay fluctuations, we show that for a suspension of pushers, bend fluctuations mediate instability and for a suspension of pullers it is splay fluctuation that initiates instability. Intuitional arguments can provide more insights into the instability of the polar phase. Figure 5(left) shows a regular collection of pushers with polar order. A small bend fluctuation is introduced to this collection by distorting the director of five selected swimmers. For a regular system, fluid velocity due to the other swimmers averages to zero at the position of each swimmer, but for the distorted case shown in this figure, fluid velocity has a non-zero value at the position of distorted swimmers. As shown by the large arrows, the velocity streamlines at the position of distorted swimmers are in the direction that tends to increase the initial distortions and destroy the initial regular state. Figure 5(right) shows the case for pullers with a small splay fluctuation. For pullers, when a small splay fluctuation is introduced, the system tends to increase it and destroy the polar order.

J. Stat. Mech. (2018) 023201

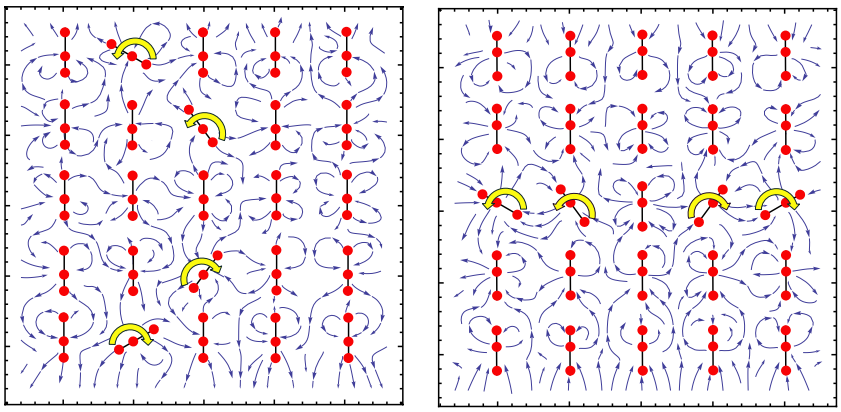

Figure 5. Flow patterns for demonstrating bend (left) and splay (right) distortions in the polarized phase. An ordered suspension of pushers (pullers) is unstable due to the growth of bend (splay) fluctuations. Small arrows show the direction of the flow field in the interparticle regions and large arrows show the flow field calculated at the position of distorted swimmers.

Another interesting feature of active nematics is the appearance of bands in the polar state. In symmetry-broken polar phase, density waves appear. The imaginary parts in equations (86), (88) and (95) reflect this fact. Interestingly, in the case of splay fluctuations, a single group velocity for these traveling waves is seen. Finally, we should mention that all instabilities arising from hydrodynamic interactions apply only to dipolar swimmers. For a collection of neutral swimmers with quadrupolar force distributions, the terms proportional to b_1 in equations (47) and (48) do not contribute and all ordered phases are stable with respect to long-wavelength fluctuations.

Acknowledgments

Useful discussions with M C Marchetti and K Kruse are acknowledged.

Appendix A. Hydrodynamic center and diffusion coefficients for a rigid swimmer

Here we want to show how the hydrodynamic center and diffusion coefficients for a swimmer can be calculated. Let us consider a rigid swimmer composed of three spheres with equal radii a, linked linearly by two negligible-diameter linkers. With the spheres labeled f, m and b, the front linkage has a length given by $L^{\mathrm{f}} = \ell$ and the back linkage has a length given by $L^{\mathrm{b}} = \ell(1+\delta)$. The hydrodynamic center for this rigid system is a point around which the translational motion is independent of the rotational motion. As a result of symmetry, for our three linearly linked spheres, the hydrodynamic center lies somewhere on the longer linkage with distance x from the middle sphere. The hydrodynamic center is a geometrical concept and it is independent of dynamics, but it can benefit any dynamical problem to calculate it. Let us consider a dynamical problem where, as a result of an external force, the hydrodynamic center moves linearly without any net rotation. With respect to the hydrodynamic center, the total torque should vanish: $x f_{\perp}^{\mathrm{m}} + (\ell + x)\, f_{\perp}^{\mathrm{f}} - (\ell(1+\delta) - x)\; f_{\perp}^{\mathrm{b}} = 0$, where $\perp$ denotes the components of vectors perpendicular to the linkages. In addition to this condition, there is a set of

J. Stat. Mech. (2018) 023201

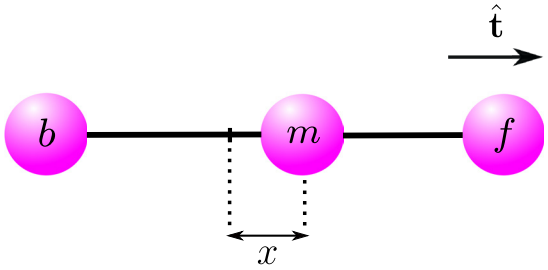

Figure A1. In an asymmetric three-sphere swimmer, the hydrodynamic center is located at distance x from the middle sphere.

linear equations that relate the forces and velocities: $\mathbf{v}^{\alpha} = \sum_{\beta=\mathrm{f},m,b} O^{\alpha\beta}\mathbf{f}^{\beta}$, where O denotes Oseen's tensor. We can use this set of equations and find relations between the perpendicular components of the forces and velocities. The rigidity condition is another equation that we must consider: $v_{\perp}^{\mathrm{f}} = v_{\perp}^{\mathrm{m}} = v_{\perp}^{\mathrm{b}}$. Using the rigidity and force–velocity equations we can obtain relations for $f_{\perp}^{\mathrm{f}}/f_{\perp}^{\mathrm{m}}$ and $f_{\perp}^{\mathrm{b}}/f_{\perp}^{\mathrm{m}}$ and plugging them into the torque-free condition, we can obtain the following result for x:

$$x = \frac{1}{3}\delta\left(\ell + \frac{7}{8}a\right). \tag{A.1}$$

Having obtained the position of the hydrodynamic center, we can now calculate the translational and rotational diffusion coefficients. To obtain the translational diffusion coefficients, let us apply an external force $\mathbf{f}_{\mathrm{T}}$ to the system and calculate the linear velocity $\mathbf{v}_{\mathrm{T}}$ that the system will acquire. Then the translational diffusion matrix $\mathbf{D}$ is defined by $\mathbf{v}_{\mathrm{T}} = (k_{\mathrm{B}}T)^{-1}\mathbf{D}\cdot\mathbf{f}_{\mathrm{T}}$. To calculate $\mathbf{D}$, one should note that in addition to force–velocity relations, constraints of the total force $\mathbf{f}^{\mathrm{f}} + \mathbf{f}^{\mathrm{m}} + \mathbf{f}^{\mathrm{b}} = \mathbf{f}_{\mathrm{T}}$ and rigidity $\mathbf{v}^{\mathrm{f}} = \mathbf{v}^{\mathrm{m}} = \mathbf{v}^{\mathrm{b}} = \mathbf{v}_{\mathrm{T}}$ should be considered. Solving these equations yields

$$(k_{\mathrm{B}}T)^{-1}D_{ij} = K(\ell)\,\hat{t}_i\hat{t}_j + K(2\ell)\,\left(\delta_{ij} - \hat{t}_i\hat{t}_j\right), \tag{A.2}$$

where

$$K(\ell) = \frac{1}{18\pi\eta a}\left[1 + \frac{5}{2}\left(1 - \frac{\delta}{2}\right)\left(\frac{a}{\ell}\right) + \mathcal{O}\left(\frac{a}{\ell}\right)^2\right]. \tag{A.3}$$

In terms of their parallel and perpendicular components, the diffusion coefficients are given by: $D_{\parallel} = k_{\mathrm{B}}TK(\ell)$ and $D_{\perp} = k_{\mathrm{B}}TK(2\ell)$.

To calculate the rotational diffusion coefficient, we apply an external torque τ around the hydrodynamic center; then the system rotates with angular velocity Ω around that center with no translation for the hydrodynamic center. Rotational diffusion can be calculated as: $\Omega = (k_{\mathrm{B}}T)^{-1}D_{\mathrm{R}}\,\tau$. In this case, in addition to the linear force–velocity relations given by Oseen's tensor, we must consider the torque equation as $\tau = xf_{\perp}^{\mathrm{m}} + (\ell + x)\,f_{\perp}^{\mathrm{f}} - (\ell(1+\delta) - x)\;f_{\perp}^{\mathrm{b}}$ and the rigidity constraints as $v_{\perp}^{\mathrm{m}} = x\Omega$, $v_{\perp}^{\mathrm{f}} = (\ell + x)\Omega$ and $v_{\perp}^{\mathrm{b}} = -\left(\ell(1+\delta) - x\right)\Omega$. Solving all these equations simultaneously yields the final result:

$$D_{\mathrm{R}} = \frac{k_{\mathrm{B}}T}{12\pi\eta a\,\ell^2}\left[(1-\delta) - \frac{3}{8}\left(1 - \frac{3}{2}\delta\right)\left(\frac{a}{\ell}\right) + \mathcal{O}\left(\frac{a}{\ell}\right)^2\right]. \tag{A.4}$$

Appendix B. Hydrodynamic interactions: alternative representation

To gain better insight into long-range hydrodynamic interactions, we provide here an alternative representation for the terms in equations (10) to (15). With the help of hydrodynamic singularities derived from the point source (or sink) and point force, vectors $\mathbf{G}_1, \cdots, \mathbf{G}_6$ can be re-written as:

$$\mathbf{G}_1 = R^2\, D^{\mathrm{f}}_{ijk}\, \hat{t}_j{}'\hat{t}_k{}', \tag{B.1}$$

$$\mathbf{G}_2 = \frac{R^3}{2}\, Q^{\mathrm{f}}_{ijkl}\, \hat{t}_j{}'\hat{t}_k{}'\hat{t}_l{}' + 3R^3\, D^{\mathrm{s}}_{jk}\, \hat{t}_i{}'\hat{t}_j{}'\hat{t}_k{}', \tag{B.2}$$

$$\mathbf{G}_3 = R^3\, Q^{\mathrm{f}}_{ijkl}\, \hat{t}_j{}'\hat{t}_k{}'\hat{t}_l, \tag{B.3}$$

$$\mathbf{G}_4 = R^3\, Q^{\mathrm{f}}_{ijkl}\, \hat{t}_j{}'\hat{t}_k{}'\hat{t}_l + 3R^3\, D^{\mathrm{s}}_{jk}\, \hat{t}_i\hat{t}_j{}'\hat{t}_k{}', \tag{B.4}$$

$$\mathbf{G}_5 = \frac{1}{2}R^4\, C^{\mathrm{f}}_{ijklm}\, \hat{t}_j{}'\hat{t}_k{}'\hat{t}_l{}'\hat{t_m} - \frac{3}{2}R^4\, Q^{\mathrm{s}}_{jkl}\, \hat{t}_j{}'\hat{t}_k{}'\hat{t}_l{}'\hat{t}_i, \tag{B.5}$$

$$\mathbf{G}_6 = \frac{1}{2}R^4\, C^{\mathrm{f}}_{ijklm}\, \hat{t}_j{}'\hat{t}_k{}'\hat{t}_l\hat{t_m} - 3R^4\, Q^{\mathrm{s}}_{jkl}\, \hat{t}_j{}'\hat{t}_k{}'\hat{t}_l\hat{t}_i, \tag{B.6}$$

where $\mathbf{D}^{\mathrm{f}}$ and $\mathbf{D}^{\mathrm{s}}$ are the force and source dipoles, $\mathbf{Q}^{\mathrm{f}}$ and $\mathbf{Q}^{\mathrm{s}}$ are the force and source quadrupole tensors, and $\mathbf{C}^{\mathrm{f}}$ represents a force octupole tensor. In terms of Oseen's tensor O_{ij}, which shows the flow field of a point force in an inertialess condition, and tensor M_{ij} (defined before), the higher-order singularities can be expressed as:

$$D^{\mathrm{f}}_{ijk} = \partial_k O_{ij}, \tag{B.7}$$

$$D^{\mathrm{s}}_{ij} = -\frac{1}{R^3} M_{ij}, \tag{B.8}$$

$$Q^{\mathrm{f}}_{ijkl} = \partial_l D^{\mathrm{f}}_{ijk}, \tag{B.9}$$

$$Q^{\mathrm{s}}_{ijk} = \partial_k D^{\mathrm{s}}_{ij}, \tag{B.10}$$

$$C^{\mathrm{f}}_{ijklm} = \partial_m Q^{\mathrm{f}}_{ijkl}. \tag{B.11}$$

Equation (B.1) shows that the term proportional to $a_1 \times \mathbf{G}_1$ in equation (7) is actually the velocity field due to a force dipole located at the position of the second swimmer and calculated at the position of the first swimmer. This force dipole is located along the direction parallel to $\hat{\mathbf{t}}'$. A similar treatment for all other terms in equations (7) and (8) can be obtained by the above representation. The details of the above equations show how different singularities are arranged with respect to vectors $\hat{\mathbf{t}}$, $\hat{\mathbf{t}}'$ and

$\hat{\mathbf{R}}$. Denoting the force dipole, force quadrupole and source dipole by $\leftarrow\!\!\rightarrow$, $\leftarrow\!\!\updownarrow\!\!\rightarrow$ and $\pm$ respectively, the hydrodynamic interactions (equations (7) and (8)) can be written symbolically as:

$$\begin{aligned}\mathbf{V}^{\mathrm{L}} &\equiv a_1[\leftarrow\!\!\rightarrow] + a_2[\pm,\ \ \leftarrow\!\!\updownarrow\!\!\rightarrow] + a_3[\leftarrow\!\!\updownarrow\!\!\rightarrow],\\ \mathbf{\Omega}^{\mathrm{L}} &\equiv a_4[\pm,\ \ \leftarrow\!\!\updownarrow\!\!\rightarrow] + a_5[\cdots] + a_6[\cdots],\end{aligned} \tag{B.12}$$

where $[\cdots]$ denotes higher-order singularities like source quadrupoles and force octupoles.

Appendix C. Details of interaction terms

In this appendix we give the details of the interaction contributions introduced in equations (56)–(58). The interaction contributions to the dynamics of the density, polarization and nematic-order parameter read as:

$$\dot{\rho}^{\mathrm{L}} = -\partial_i \left(\left[b_1\, T_i^1 + b_2\, T_i^2 \right]\ \rho + b_3\, T_{il}^3\, \rho\, P_l \right), \tag{C.1}$$

$$\dot{\rho}^{\mathrm{S}} = -\frac{4}{3}\pi \ell_{\mathrm{c}}^3 U_0 \partial_i \Bigg(\rho\, \partial_j(\rho P_k) \Bigg(\frac{1}{5} D_2 \left(\delta_{kj} P_i + \delta_{ik} P_j + \delta_{ij} P_k \right) + D_\perp \delta_{ij} P_k \Bigg) \Bigg), \tag{C.2}$$

$$\begin{aligned}\dot{P}_i^{\mathrm{L}} =& -\partial_j \left(\left(b_1\, T_j^1 + b_2\, T_j^2 \right) \rho\, P_i + b_3\, T_{jl}^3\, \rho \left(N_{il} + \frac{\delta_{il}}{3} \right) \right)\\ &+ \frac{4}{5} \left(b_1 T_{il}^4 - b_2 T_{il}^5 \right) \rho P_l - \frac{1}{5} b_1 T_{ll}^4\, \rho P_i + \frac{6}{7} b_4 T_{ilm}^6\, \rho N_{lm}\\ &- \frac{1}{5} \left(b_1 T_{li}^4 - b_2 T_{li}^5 \right) \rho P_l - \frac{2}{7} b_4 T_{mlm}^6\, \rho N_{li} - \frac{18}{35} b_4 T_{lli}^6\, \rho\\ &- \frac{2}{7} b_4 T_{lim}^6\, \rho N_{lm},\end{aligned} \tag{C.3}$$

$$\begin{aligned}\dot{P}_i^{\mathrm{S}} =& -\frac{4}{3}\pi \ell_{\mathrm{c}}^3\, U_0\, \partial_j \Bigg(D_2\, \frac{\rho}{7} \Bigg(\frac{7}{15} \left[\partial_i(\rho P_j) + \partial_j(\rho P_i) + \delta_{ij} \boldsymbol{\nabla} \cdot (\rho \mathbf{P}) \right]\\ &+ \partial_k(\rho P_j) N_{ik} + \partial_j(\rho P_l) N_{li} + \partial_k(\rho P_i) N_{kj} + \boldsymbol{\nabla} \cdot (\rho \mathbf{P}) N_{ij}\\ &+ \partial_k(\rho P_l) N_{lk}\, \delta_{ij} + \partial_i(\rho P_l) N_{lj} \Bigg) + D_\perp \rho \left(\partial_j(\rho P_l) N_{li} + \frac{1}{3} \partial_j(\rho P_i) \right) \Bigg)\\ &+ \frac{4}{3}\pi D_{\mathrm{R}} \ell_{\mathrm{c}}^3 U_0 \rho^2 \left(\frac{2}{3} P_i - P_j N_{ij} \right),\end{aligned} \tag{C.4}$$

J. Stat. Mech. (2018) 023201

$$
\begin{aligned}
\dot{N}^{\mathrm{L}}_{ij} =& -\boldsymbol{\nabla}.\left[\left(b_1\mathbf{T}^1+b_2\,\mathbf{T}^2\right)\rho N_{ij}\right]\\
&-\frac{1}{5}b_3\partial_z\left(T^3_{zj}\rho P_i+T^3_{zi}\rho P_j-\frac{2}{3}\delta_{ij}T^3_{zl}\rho P_l\right)\\
&+\frac{\rho}{7}\Bigg(\frac{7}{5}\left[b_1(T^4_{ij}+T^4_{ji})-b_2(T^5_{ij}+T^5_{ji})\right]+5b_1T^4_{il}\,N_{jl}\\
&-\frac{14}{15}b_1T^4_{ll}\,\delta_{ij}-2b_1T^4_{li}\,N_{lj}-3b_2T^5_{il}N_{lj}-2b_1T^4_{lj}N_{li}+5b_1T^4_{jl}N_{li}\\
&-3b_2T^5_{lj}N_{li}-2b_1T^4_{ll}N_{ij}-2\left[b_1T^4_{ml}-b_2T^5_{ml}\right]N_{ml}\delta_{ij}\Bigg)\\
&+\frac{4}{315}b_4\rho\Bigg(-9T^6_{lli}P_j+26T^6_{ijl}P_l-9T^6_{llj}P_i-9T^6_{llm}P_m\delta_{ij}\\
&+26T^6_{jil}P_l-9T^6_{lij}P_l\Bigg),
\end{aligned}
\tag{C.5}
$$

$$
\begin{aligned}
\dot{N}^{\mathrm{S}}_{ij} =& -\frac{4}{3}\pi\ell_{\mathrm{c}}^3\,U_0\,\partial_k\Bigg(\rho\Bigg(\frac{1}{35}D_2\Bigg(\partial_l(\rho P_l)P_i\,\delta_{jk}+\partial_l(\rho P_l)P_j\,\delta_{ik}\\
&-\frac{4}{3}\left(\partial_l(\rho P_l)P_k+\partial_l(\rho P_k)P_l\right)\delta_{ij}+\partial_l(\rho P_i)P_l\,\delta_{jk}\\
&+\partial_l(\rho P_j)P_l\,\delta_{ik}+\partial_i(\rho P_m)P_m\,\delta_{jk}+\partial_j(\rho P_m)P_m\,\delta_{ik}\\
&+(\partial_j(\rho P_i)+\partial_i(\rho P_j))P_k+\partial_j(\rho P_k)P_i+\partial_i(\rho P_k)P_j\Bigg)\\
&-\frac{2}{21}D_5\,\partial_k(\rho P_l)P_l\,\delta_{ij}+\frac{1}{5}D_4\,\partial_k\left[(\rho P_i)P_j+(\rho P_j)P_i\right]\Bigg)\Bigg)\\
&+\frac{8}{5}\pi D_{\mathrm{R}}\ell_{\mathrm{c}}^3U_0\rho^2\left(P_iP_j-\frac{P^2}{3}\,\delta_{ij}\right).
\end{aligned}
\tag{C.6}
$$

In sections 4.2 and 4.3, where we study the linear stability of the isotropic and polar phases, we need to linearize the interaction contributions. Here we briefly present the details of such calculations for a typical term. Let us consider the first term of $\dot{\rho}^{\mathrm{L}}$ in density equation (C.1). We have:

$$
-b_1\partial_i\left(T^1_i\rho\right)=-b_1\partial_i\left(\int \mathrm{d}\mathbf{r}'\frac{\hat{R}_i}{R^2}M_{jk}(\hat{\mathbf{R}})\rho(\mathbf{r}')N_{jk}(\mathbf{r}')\rho(\mathbf{r})\right),
\tag{C.7}
$$

where $\mathbf{R}=\mathbf{r}-\mathbf{r}'$. Now we can substitute the isotropic values of ρ and $\mathbf{N}$ from (67) and (69) into (C.7). Taking the spatial Fourier transform and defining $W_{ijk}=\frac{\hat{R}_i}{R^2}M_{jk}$, we have:

$$
\begin{aligned}
-b_1\partial_i\left(T_i^1\rho\right) &= -b_1\rho_0^2\,\partial_i\left(\int \mathrm{d}\mathbf{r}'\int \mathrm{d}\mathbf{k}\mathrm{e}^{-\mathrm{i}\mathbf{k}\cdot(\mathbf{r}-\mathbf{r}')}\check{W}_{ijk}(\mathbf{k})\int \mathrm{d}\mathbf{k}'\mathrm{e}^{-\mathrm{i}\mathbf{k}'\cdot\mathbf{r}'}\delta\check{N}_{jk}(\mathbf{k}')\right)\\
&= -b_1\rho_0^2\,\partial_i\left(\int \mathrm{d}\mathbf{k}\int \mathrm{d}\mathbf{k}'\delta(\mathbf{k}-\mathbf{k}')\check{W}_{ijk}(\mathbf{k})\mathrm{e}^{-\mathrm{i}\mathbf{k}\cdot\mathbf{r}}\delta\check{N}_{jk}(\mathbf{k}')\right)\\
&= \mathrm{i}b_1\rho_0^2\left(\int \mathrm{d}\mathbf{k}\mathrm{e}^{-\mathrm{i}\mathbf{k}\cdot\mathbf{r}}\,k_i\,\check{W}_{ijk}(\mathbf{k})\delta\check{N}_{jk}(\mathbf{k})\right). \qquad \text{(C.8)}
\end{aligned}
$$

To proceed further, we need to calculate the Fourier transform of W_{ijk}. As a result of symmetry, the following general expression for $\check{W}_{ijk}$ can be written:

$$\check{W}_{ijk} = A\hat{k}_i\hat{k}_j\hat{k}_k + B\hat{k}_i\delta_{jk} + C\hat{k}_j\delta_{ik} + D\hat{k}_k\delta_{ij}, \qquad \text{(C.9)}$$

where scalar functions A, B, C and D can depend on k and the Fourier transform is defined by:

$$\check{W}_{ijk} = \int \mathrm{d}\mathbf{R}\,\mathrm{e}^{\mathrm{i}\mathbf{k}\cdot\mathbf{R}}\,W_{ijk}(\mathbf{R}). \qquad \text{(C.10)}$$

Multiplying the above two equations by $\hat{k}_i\hat{k}_j\hat{k}_k$, $\hat{k}_i\delta_{jk}$, $\hat{k}_j\delta_{ik}$ and $\hat{k}_k\delta_{ij}$, we obtain the following four equations for unknown functions:

$$A + B + C + D = \int \mathrm{d}\mathbf{R}\,\mathrm{e}^{\mathrm{i}\mathbf{k}\cdot\mathbf{R}}\frac{1}{R^2}\left((\hat{\mathbf{k}}\cdot\hat{\mathbf{R}})^3 - \frac{1}{3}(\hat{\mathbf{k}}\cdot\hat{\mathbf{R}})\right), \qquad \text{(C.11)}$$

$$A + 3B + C + D = 0, \qquad \text{(C.12)}$$

$$A + B + 3C + D = \frac{2}{3}\int \mathrm{d}\mathbf{R}\,\mathrm{e}^{\mathrm{i}\mathbf{k}\cdot\mathbf{R}}\frac{1}{R^2}(\hat{\mathbf{k}}\cdot\hat{\mathbf{R}}), \qquad \text{(C.13)}$$

$$A + B + C + 3D = \frac{2}{3}\int \mathrm{d}\mathbf{R}\,\mathrm{e}^{\mathrm{i}\mathbf{k}\cdot\mathbf{R}}\frac{1}{R^2}(\hat{\mathbf{k}}\cdot\hat{\mathbf{R}}). \qquad \text{(C.14)}$$

By evaluating the integrals, we can obtain the following result for $\check{W}_{ijk}$:

$$\check{W}_{ijk} = -\frac{8\pi\mathrm{i}}{3k}\hat{k}_i\hat{k}_j\hat{k}_k + \frac{4\pi\mathrm{i}}{3k}\hat{k}_j\delta_{ik} + \frac{4\pi\mathrm{i}}{3k}\hat{k}_k\delta_{ij}. \qquad \text{(C.15)}$$

With a similar procedure, all other interaction integrals can be calculated.

References

[1] Toner J, Tu Y and Ramaswamy S 2005 Hydrodynamics and phases of flocks *Ann. Phys.* **318** 170–244
[2] Marchetti M C, Joanny J F, Ramaswamy S, Liverpool T B, Prost J, Rao M and Simha R A 2013 Hydrodynamics of soft active matter *Rev. Mod. Phys.* **85** 1143
[3] Vicsek T and Zafeiris A 2012 Collective motion *Phys. Rep.* **517** 71–140
[4] Ramaswamy S 2017 Active matter *J. Stat. Mech.* 054002
[5] Becco C, Vandewalle N, Delcourt J and Poncin P 2006 Experimental evidences of a structural and dynamical transition in fish school *Physica* A **367** 487–93
[6] Cavagna A *et al* 2015 Flocking and turning: a new model for self-organized collective motion *J. Stat. Phys.* **158** 601–27
[7] Nagy M, Akos Z, Biro D and Vicsek T 2010 Hierarchical group dynamics in pigeon flocks *Nature* **464** 890–3

J. Stat. Mech. (2018) 023201

[8] Peruani F, Starruß J, Jakovljevic V, S-Andersen L, Deutsch A and Bär M 2012 Collective motion and nonequilibrium cluster formation in colonies of gliding bacteria *Phys. Rev. Lett.* **108** 098102
[9] Tokita R, Katoh T, Maeda Y, Wakita J-I, Sano M, Matsuyama T and Matsushita M 2009 Pattern formation of bacterial colonies by *Escherichia coli* *J. Phys. Soc. Japan* **78** 074005
[10] Lushi E, Wioland H and Goldstein R E 2014 Fluid flows created by swimming bacteria drive self-organization in confined suspensions *Proc. Natl Acad. Sci.* **111** 9733–8
[11] Sokolov A, Aranson I S, Kessler J O and Goldstein R E 2007 Concentration dependence of the collective dynamics of swimming bacteria *Phys. Rev. Lett.* **98** 158102
[12] Prost J, Jülicher F and Joanny J F 2015 Active gel physics *Nat. Phys.* **11** 111–7
[13] Theurkauff I, Cottin-Bizonne C, Palacci J, Ybert C and Bocquet L 2012 Dynamic clustering in active colloidal suspensions with chemical signaling *Phys. Rev. Lett.* **108** 268303
[14] Buttinoni I, Bialké J, Kümmel F, Löwen H, Bechinger C and Speck T 2013 Dynamical clustering and phase separation in suspensions of self-propelled colloidal particles *Phys. Rev. Lett.* **110** 238301
[15] Bayati P and Najafi A 2016 Dynamics of two interacting active Janus particles *J. Chem. Phys.* **144** 134901
[16] Schaller V, Weber C, Semmrich C, Frey E and Bausch A R 2010 Polar patterns of driven filaments *Nature* **467** 73–7
[17] Sumino Y, Nagai K H, Shitaka Y, Tanaka D, Yoshikawa K, Chaté H and Oiwa K 2012 Large-scale vortex lattice emerging from collectively moving microtubules *Nature* **483** 448–52
[18] Narayan V, Ramaswamy S and Menon N 2007 Long-lived giant number fluctuations in a swarming granular nematic *Science* **317** 105–8
[19] Mermin N D and Wagner H 1966 Absence of ferromagnetism or antiferromagnetism in one or two-dimensional isotropic Heisenberg models *Phys. Rev. Lett.* **17** 1133
[20] Toner J and Tu Y 1995 Long-range order in a two-dimensional dynamical XY model: how birds fly together *Phys. Rev. Lett.* **75** 4326
[21] Saintillan D and Shelley M J 2008 Instabilities, pattern formation and mixing in active suspensions *Phys. Fluids* **20** 123304
[22] Whitfield C A, Adhyapak T C, Tiribocchi A, Alexander G P, Marenduzzo D and Ramaswamy S 2017 Hydrodynamic instabilities in active cholesteric liquid crystals *Eur. Phys. J.* E **40** 50
[23] Oyama N, Molina J J and Yamamoto R 2017 Simulations of model microswimmers with fully resolved hydrodynamics *J. Phys. Soc. Japan* **86** 101008
[24] Genkin M M, Sokolov A, Lavrentovich O D and Aranson I S 2017 Topological defects in a living nematic ensnare swimming bacteria *Phys. Rev.* X **7** 011029
[25] Ramaswamy S and Rao M 2007 Active-filament hydrodynamics: instabilities, boundary conditions and rheology *New J. Phys.* **9** 423
[26] Zöttl A and Stark H 2014 Hydrodynamics determines collective motion and phase behavior of active colloids in quasi-two-dimensional confinement *Phys. Rev. Lett.* **112** 118101
[27] Hohenegger C and Shelley M J 2010 Stability of active suspensions *Phys. Rev.* E **81** 046311
[28] Liverpool T B and Marchetti M C 2003 Instabilities of isotropic solutions of active polar filaments *Phys. Rev. Lett.* **90** 138102
[29] Ahmadi A, Marchetti M C and Liverpool T B 2006 Hydrodynamics of isotropic and liquid crystalline active polymer solutions *Phys. Rev.* E **74** 061913
[30] Peshkov A, Bertin E, Ginelli F and Chaté H 2014 Boltzmann–Ginzburg–Landau approach for continuous descriptions of generic Vicsek-like models *Eur. Phys. J. Spec. Top.* **223** 1315
[31] Ihle T 2011 Kinetic theory of flocking: derivation of hydrodynamic equations *Phys. Rev.* E **83** 030901
[32] Baskaran A and Marchetti M C 2009 Statistical mechanics and hydrodynamics of bacterial suspensions *Proc. Natl Acad. Sci.* **106** 15567
[33] Blaschke J, Maurer M, Menon K, Zöttl A and Stark H 2016 Phase separation and coexistence of hydrodynamically interacting microswimmers *Soft Matter* **12** 9821–31
[34] Saintillan D and Shelley M J 2008 Instabilities and pattern formation in active particle suspensions: kinetic theory and continuum simulations *Phys. Rev. Lett.* **100** 178103
[35] Behmadi H, Fazli Z and Najafi A 2017 A 2D suspension of active agents: the role of fluid mediated interaction *J. Phys.: Condens. Matter* **29** 115102
[36] Grégoire G and Chaté H 2004 Onset of collective and cohesive motion *Phys. Rev. Lett.* **92** 025702
[37] Chaté H, Ginelli F, Grégoire G and Raynaud F 2008 Collective motion of self-propelled particles interacting without cohesion *Phys. Rev.* E **77** 046113
[38] Peruani F, Deutsch A and Bär M 2006 Nonequilibrium clustering of self-propelled rods *Phys. Rev.* E **74** 030904
[39] Vicsek T, Czirók A, Ben-Jacob E, Cohen I and Shochet O 1995 Novel type of phase transition in a system of self-driven particles *Phys. Rev. Lett.* **75** 1226

J. Stat. Mech. (2018) 023201

[40] Chaté H, Ginelli F, Grégoire G, Peruani F and Raynaud F 2008 Modeling collective motion: variations on the Vicsek model *Eur. Phys. J.* B **64** 451–6
[41] Baskaran A and Marchetti M C 2008 Enhanced diffusion and ordering of self-propelled rods *Phys. Rev. Lett.* **101** 268101
[42] Bertin E, Droz M and Grégoire G 2009 Hydrodynamic equations for self-propelled particles: microscopic derivation and stability analysis *J. Phys. A: Math. Theor.* **42** 445001
[43] Toner J and Tu Y 1998 Flocks, herds and schools: a quantitative theory of flocking *Phys. Rev.* E **58** 4828
[44] Ramaswamy S and Simha R A 2002 Hydrodynamic fluctuations and instabilities in ordered suspensions of self-propelled particles *Phys. Rev. Lett.* **89** 058101
[45] Mishra S, Baskaran A and Marchetti M C 2010 Fluctuations and pattern formation in self-propelled particles *Phys. Rev.* E **81** 061916
[46] Leoni M and Liverpool T B 2010 Swimmers in thin films: from swarming to hydrodynamic instabilities *Phys. Rev. Lett.* **105** 238102
[47] Purcell E M 1977 Life at low Reynolds number *Am. J. Phys.* **45** 3–11
[48] Najafi A and Golestanian R 2005 Propulsion at low Reynolds number *J. Phys.: Condens. Matter* **17** S1203
[49] Zargar R, Najafi A and Miri M F 2009 Three-sphere low-Reynolds-number swimmer near a wall *Phys. Rev.* E **80** 026308
[50] Pozrikidis C 1992 *Boundary Integral and Singularity Methods for Linearized Viscous Flow* (Cambridge: Cambridge University Press)
[51] Moradi M and Najafi A 2015 Rheological properties of a dilute suspension of self-propelled particles *Europhys. Lett.* **109** 24001
[52] Farzin M, Ronasi K and Najafi A 2012 General aspects of hydrodynamic interactions between three-sphere low Reynolds number swimmers *Phys. Rev.* E **85** 061914
[53] Alexander G P, Pooley C M and Yeomans J M 2009 Hydrodynamics of linked sphere model swimmers *J. Phys.: Condens. Matter* **21** 204108
[54] Lauga E and Powers T R 2009 The hydrodynamics of swimming microorganisms *Rep. Prog. Phys.* **72** 096601
[55] Elgeti J, Winkler R G and Gompper G 2015 Physics of microswimmers—single particle motion and collective behavior: a review *Rep. Prog. Phys.* **78** 056601
[56] Drescher K, Goldstein R E, Michel N, Polin M and Tuval I 2010 Direct measurement of the flow field around swimming microorganisms *Phys. Rev. Lett.* **105** 168101
[57] Najafi A and Golestanian R 2010 Coherent hydrodynamic coupling for stochastic swimmers *Europhys. Lett.* **90** 68003
[58] Kim S and Karrila S J 2005 *Microhydrodynamics: Principles and Selected Applications* (New York: Dover)
[59] Happel J and Brenner H 1965 *Low Reynolds Number Hydrodynamics with Special Applications to Particulate Media* (Englewood Cliffs, NJ: Prentice-Hall)
[60] Yoshinaga N and Liverpool T B 2017 Hydrodynamic interactions in dense active suspensions: from polar order to dynamical clusters *Phys. Rev.* E **96** 020603
[61] Howse J R, Jones R A L, Ryan A J, Gough T, Vafabakhsh R and Golestanian R 2007 Self-motile colloidal particles: from directed propulsion to random walk *Phys. Rev. Lett.* **99** 048102
[62] Baskaran A and Marchetti M C 2008 Hydrodynamics of self-propelled hard rods *Phys. Rev.* E **77** 011920

J. Stat. Mech. (2018) 023201